Nonsense mediated decay and a novel protein Period-2 regulate *casein kinase I* in an opposing manner to control circadian period in *Neurospora crassa*

Christina M. Kelliher[1], Randy Lambreghts[1], Qijun Xiang[1], Christopher L. Baker[1,3], Jennifer J. Loros[2], and Jay C. Dunlap[1,*]

[1] Department of Molecular & Systems Biology, Geisel School of Medicine at Dartmouth, Hanover, NH, USA

[2] Department of Biochemistry & Cell Biology, Geisel School of Medicine at Dartmouth, Hanover, NH, USA

[3] Genetics and Genomics, The Jackson Laboratory, Bar Harbor, ME, 04660, USA

* Corresponding author

Email: jay.c.dunlap@dartmouth.edu

Keywords: Circadian Clock, *Neurospora crassa*, Casein Kinase I, Period-2, Period-6, Nonsense Mediated Decay, RNA-binding protein, RNA stability

Abstract

Circadian clocks in fungi and animals are driven by a functionally conserved transcription-translation feedback loop. In *Neurospora crassa*, negative feedback is executed by a complex of Frequency (FRQ), FRQ-interacting RNA helicase (FRH), and Casein Kinase I (CKI), which inhibits the activity of the clock's positive arm, the White Collar Complex (WCC). Here, we show that the *period-2* gene, whose mutation is characterized by recessive inheritance of a long 26-hour period phenotype, encodes an RNA-binding protein that stabilizes the *ck-1a* transcript, resulting in CKI protein levels sufficient for normal rhythmicity. Moreover, by examining the molecular basis for the short circadian period of *period-6* mutants, we uncovered a strong influence of the Nonsense Mediated Decay pathway on CKI levels. The finding that circadian period defects in two classically-derived *Neurospora* clock mutants each arise from disruption of *ck-1a* regulation is consistent with circadian period being exquisitely sensitive to levels of *casein kinase I*.

Introduction

The *Neurospora* circadian oscillator is a transcription-translation feedback loop that is positively regulated by the White Collar Complex (WCC) transcription factors, which drive expression of the negative arm component Frequency (FRQ). The circadian negative arm complex is composed of FRQ, FRQ-Interacting RNA helicase (FRH), and Casein Kinase I (CKI), which promote WCC phosphorylation on key phospho-sites to inhibit its activity (Wang et al., 2019). Although not related by sequence similarity, FRQ is functionally homologous to PERs and CRYs in the animal clock. FRQ, PERs, and CRYs are extensively regulated transcriptionally, translationally, and post-translationally over the circadian day, and these regulatory mechanisms are highly conserved among clocks in animals and fungi (reviewed in: (Hurley et al., 2016)).

Negative arm components are regulated at the RNA and protein levels to maintain circadian phase and period. Anti-sense transcription at the *frq* locus produces the *qrf* transcript, which is required for proper phase control and light responses of the fungal clock (Kramer et al., 2003). The mammalian PER2 anti-sense transcript displays nearly identical dynamics to *qrf* expression (Koike et al., 2012). PER2 sense expression levels are further regulated by microRNA binding sites in its 3' UTR (Yoo et al., 2017). In a similar manner, *frq* RNA is directly targeted for turnover by rhythmic exosome activity in the late day (Guo et al., 2009). Splicing of the *frq* transcript is regulated by temperature (Colot et al., 2005), mirroring thermal regulation mechanisms in the clocks of *Drosophila* (Majercak et al., 1999) and *Arabidopsis* (James et al.,

2012). FRQ is an intrinsically disordered protein encoded by non-optimal codons to improve its co-translational folding (Zhou et al., 2013), and FRQ structure is also stabilized by its binding partner FRH (Hurley et al., 2013). PER2 is also largely intrinsically disordered, and indeed circadian clock proteins across species have large stretches of intrinsic disorder which are in the early stages of functional characterization (Pelham et al., 2020; Pelham et al., 2018) (reviewed in: (Partch, 2020)). Finally, an extremely conserved feature of the clock's negative arm is progressive phosphorylation and alteration of function over time (reviewed in: (Dunlap and Loros, 2018)). FRQ is progressively phosphorylated over the day (Baker et al., 2009), as are CRY1 and PER2 in the mammalian oscillator (Ode et al., 2017; Vanselow et al., 2006). A conserved phospho-switch in mammalian PER2 and fly PER proteins has been implicated in both temperature compensation and in closing the circadian feedback loop (Philpott et al., 2020; Top et al., 2018). Taken together, FRQ, PERs, and CRYs are tightly regulated and underlying mechanisms are often conserved between clock models.

In contrast, less is known about the mechanisms regulating expression of the other essential member of the negative arm complex, CKI, orthologs of which are highly conserved in sequence and in function across eukaryotic clocks. CKI forms a stable complex as FRQ-FRH-CKIa in *Neurospora* (Baker et al., 2009; Gorl et al., 2001), as PER-DOUBLETIME (DBT) in flies (Kloss et al., 2001), and as a multi-protein complex of PER-CRY-CKIδ in mouse (Aryal et al., 2017). Fungal CKI phosphorylates both FRQ and WCC (He et al., 2006). Insect DBT and mammalian CKIδ/ε are key regulators of the PER2 phospho-switch, including phosphorylation of hPER2 at S662, which is associated with the human sleep and circadian disorder FASPS (Narasimamurthy et al., 2018; Philpott et al., 2020; Toh et al., 2001; Zhou et al., 2015). Significantly, mutation of human CKIδ itself phenocopies this, also leading to FASPS (Xu et al., 2005). CKI phosphorylations contribute to feedback loop closure in all species, and FRQ-CKI binding strength is a key regulator of period length in *Neurospora* (Liu et al., 2019). CKI abundance is not rhythmic in any species described to date (Gorl et al., 2001; Kloss et al., 2001), but preliminary evidence suggests that its expression levels are tightly controlled to keep the clock on time, just like FRQ/PER/CRY. In mammals, CKI knockdown or knock out significantly lengthens period (Isojima et al., 2009; Lee et al., 2009; Tsuchiya et al., 2016), and CKIδ levels are negatively regulated by m6A methylation (Fustin et al., 2018). In *Neurospora*, decreasing the amounts of the *casein kinase I* (*ck-1a*) transcript using a regulatable promoter leads to long period defects up to ~30 hours (Mehra et al., 2009). CKI has a conserved C-terminal domain involved in autophosphorylation and inhibition of kinase activity (Guo et al., 2019). Fungal mutants lacking this CKI C-terminal inhibitory domain have hyperactive kinase

activity (Querfurth et al., 2007) and display short periods. Across clock models, the circadian period is sensitive to CKI abundance and activity due to its importance in circadian feedback loop closure.

Our modern understanding of the circadian clock was founded on genetic screens and characterization of mutants with circadian defects (Feldman and Hoyle, 1973; Konopka and Benzer, 1971; Ralph and Menaker, 1988). The fungal clock model *Neurospora crassa* has been a top producer of relevant circadian mutants due to its genetic tractability, ease of circadian readout, and functional conservation with the animal circadian clock (reviewed in: (Loros, 2020)). Forward genetic screens used the *ras-1*^{bd} mutant background (which forms distinct bands of conidiophores once per subjective night) in race tube assays to identify key players in the circadian clock (Belden et al., 2007; Feldman and Hoyle, 1973; Sargent et al., 1966). Genetic epistasis among the *period* genes, and in some cases, genetic mapping of mutations was also performed using *N. crassa* (Feldman and Hoyle, 1976; Gardner and Feldman, 1981; Morgan and Feldman, 2001).

All but one of the extant *period* genes in *Neurospora* have been cloned, and their identities have expanded our knowledge of core-clock modifying processes. *period-4*, or Checkpoint Kinase 2 (Chk2), linked the clock to cell-cycle progression (Pregueiro et al., 2006). *period-3*, or Casein Kinase II (CKII), implicated direct phosphorylation of core clock proteins as central to temperature compensation (Mehra et al., 2009). *period-1* is an essential RNA-helicase that regulates the core clock under high nutrient environments (Emerson et al., 2015). *period-6* is a core subunit of the Nonsense-Mediated Decay (NMD) complex (Compton, 2003), although its circadian role remains cryptic. Among the available *period* genes, only *period-2* remains uncharacterized.

We have mapped the *period-2* mutation to NCU01019 using whole genome sequencing, and discovered its molecular identity; however, attributing its long period mutant phenotype to molecular function has remained elusive (Lambreghts, 2012). Equipped with the identity of PRD-2, we then followed up on the observation that the *prd-6* short period phenotype is completely epistatic to the *prd-2* mutant's long period (Morgan and Feldman, 1997, 2001). We find that PRD-6 and PRD-2 use distinct mechanisms to play opposing roles in regulating levels of the *casein kinase I* transcript in *Neurospora,* thus rationalizing the circadian actions of the two clock mutants whose roles in the clock were unknown. PRD-2 stabilizes the *ck-1a* mRNA transcript, and the clock-relevant domains and biochemical evaluation of the PRD-2 protein indicate that it acts as an RNA-binding protein. We genetically rescue the long period phenotype of *prd-2* mutants by expressing a hyperactive CKI allele and by titrating up *ck-1a* mRNA levels

using a regulatable promoter. The endogenous *ck-1a* transcript has a strikingly long 3' UTR, indicating that its mRNA could be subject to NMD during a normal circadian day. We confirm that *prd-6* mutants have elevated levels of *ck-1a* in the absence of NMD, and further rescue the short period defect of *prd-6* mutants by titrating down *ck-1a* mRNA levels using an inducible promoter. Taken together, a unifying model emerges to explain the action of diverse *period* mutants, where the *casein kinase I* transcript is subject to complex regulation by NMD and an RNA-binding protein, PRD-2, to control its gene expression and maintain a normal circadian period.

Results

An Interstitial Inversion Identifies *prd-2*.

Genetic mapping and preliminary analyses identified *period-2* as a recessive mutant with an abnormally long ~ 26 hour period length that mapped to the right arm of LG V (Morgan and Feldman, 1997, 2001). Genetic fine structure mapping using selectable markers flanking *prd-2*, in preparation for an anticipated chromosome walk, revealed an extensive region of suppressed recombination in the region of the gene, consistent with the existence of a chromosome inversion (Lambreghts, 2012). PCR data consistent with this prompted whole genome sequencing that revealed a 322 kb inversion on chromosome V (Lambreghts, 2012) in the original isolate strain hereafter referred to as *prd-2*^{INV}. The left breakpoint of the inversion occurs in the 5' UTR of NCU03775, and its upstream regulatory sequences are displaced in the *prd-2*^{INV} mutant. However, a knockout of NCU03775 (FGSC12475) has a wild-type circadian period length, unlike the long period *prd-2*^{INV} mutant (Supplementary Figure 1). The next closest gene upstream of the left inversion is NCU03771, but its transcription start site (TSS) is > 7 kb away. The right breakpoint of the inversion occurs in the 5' UTR of NCU01019, disrupting 333 bases of its 5' UTR and its entire promoter region (Figure 1A – B). A knockout of NCU01019 has a 26 hour long period, matching the *prd-2*^{INV} long period phenotype (Figure 1C). The *prd-2*^{INV} mutant has drastically reduced levels of NCU01019 gene expression in constant light and in the subjective evening (Figure 1D), suggesting that the inversion completely disrupts the NCU01019 promoter and TSS. Placing NCU01019 under the nutrient-responsive *qa-2* promoter, we find that the long period length occurs at very low gene expression levels using 10^{-6} M quinic acid induction (Figure 1E). Finally, ectopic expression of NCU01019 at the *csr-1* locus in the *prd-2*^{INV} background rescues the long period phenotype (Figure 1F). We conclude that PRD-2 is encoded by NCU01019.

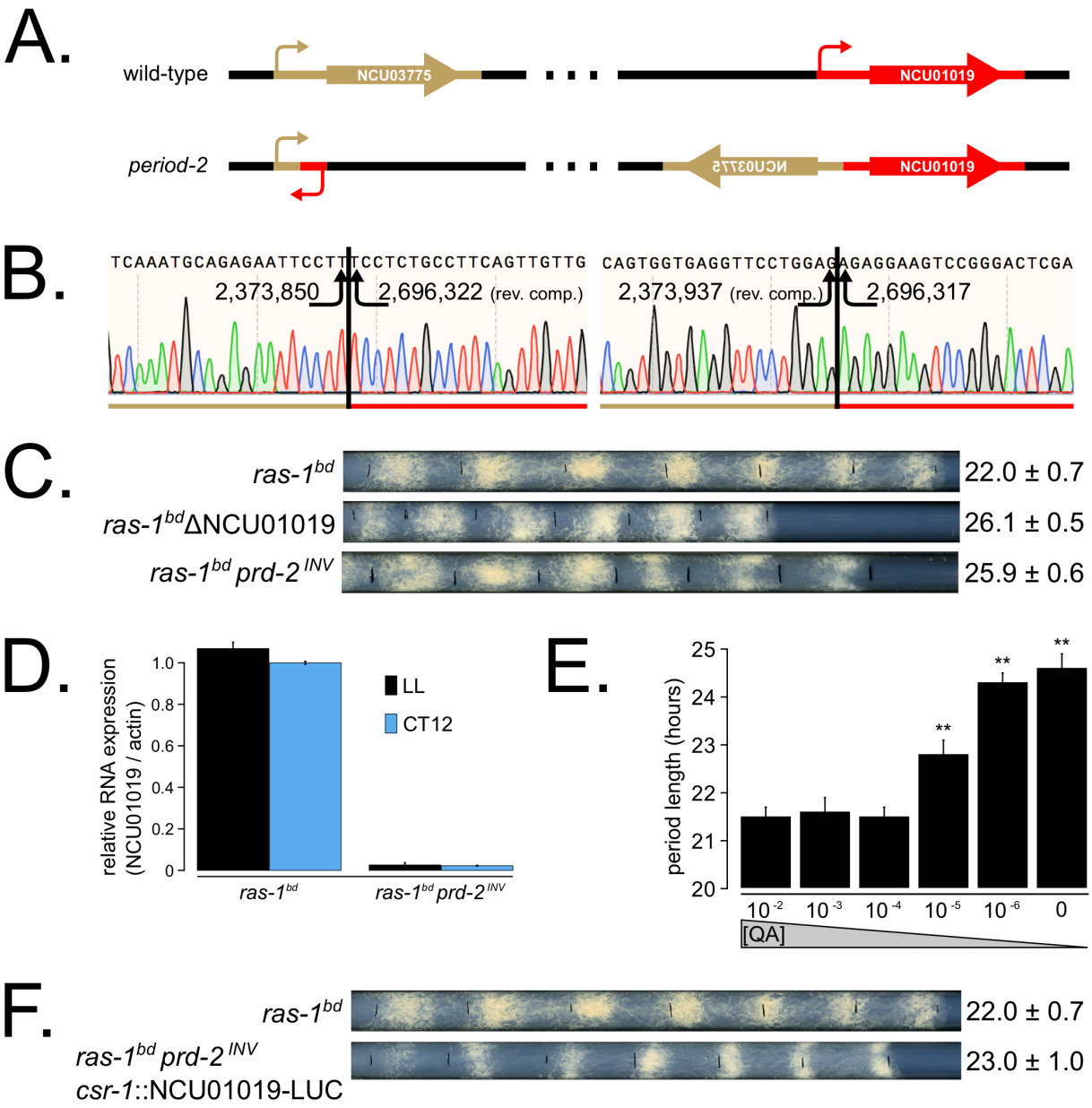

Figure 1. The *period-2* phenotype derives from reduced expression of NCU01019. Whole genome sequencing identified a 322,386 bp inversion on linkage group V in the original *period-2* mutant strain (Lambreghts, 2012). The inversion breakpoints disrupt two loci, NCU03775 and NCU01019, depicted in cartoon form (**A**). Sanger sequencing confirms the DNA sequence of the left and right breakpoints, and the corresponding NC12 genome coordinates are shown at each arrowhead (**B**). Circadian period length was determined by race tube assay for *ras-1*^{bd} controls, targeted deletion of the NCU01019 locus, and the classically derived *prd-2*^{INV} mutant.

The ΔNCU01019 mutant has a long period and slow growth defect similar to *prd-2*^{INV} (**C**). NCU01019 RNA expression levels are detectable by RT-qPCR in the *prd-2*^{INV} mutant but are drastically reduced compared to *ras-1*^{bd} controls grown in constant light or at subjective dusk CT12 (**D**). After replacing the endogenous promoter of NCU01019 with the inducible *qa-2* promoter, addition of high levels of quinic acid (10^{-2} – 10^{-3} M) led to a normal circadian period by race tube assay (10^{-2} M τ = 21.5 ± 0.2 hours; 10^{-3} M τ = 21.6 ± 0.3 hours; 10^{-4} M τ = 21.5 ± 0.2 hours). Lower levels of QA inducer led to a long circadian period (10^{-5} M τ = 22.8 ± 0.3 hours; 10^{-6} M τ = 24.3 ± 0.2 hours; 0 QA τ = 24.6 ± 0.3 hours) due to reduced NCU01019 expression. Asterisks (**) indicate $p < 1x10^{-10}$ by student's t-test compared to 10^{-2} M QA race tube results (**E**). The entire NCU01019 locus (plus 951 bases of its upstream promoter sequence) was fused in-frame with codon-optimized luciferase. Ectopic expression of this NCU01019-luc construct in the *prd-2*^{INV} background rescues the long period phenotype by race tube assay (**F**).

We mapped the clock-relevant domains of the PRD-2 protein (Figure 2A), finding that both an SUZ domain and the proline-rich C-terminus of PRD-2 are required for a normal clock period. This result was confirmed in two separate genetic backgrounds either by replacing the endogenous locus with domain deletion mutants (Figure 2B) or by ectopic expression of domain mutants at the *csr-1* locus in a Δ*prd-2* background (Figure 2C) (Supplementary Table 1). The SUZ domain family can bind RNA directly *in vitro* (Song et al., 2008), but curiously PRD-2's adjacent R3H domain, which is better characterized in the literature as a conserved RNA-binding domain, is dispensable for clock function. The C-terminus of PRD-2 is predicted to be highly disordered, and finer mapping of this region showed that neither a glutamine/proline-rich domain (amino acids 525 – 612, 21% Gln, 26% Pro) nor a domain conserved across fungal orthologs (amino acids 625 – 682, 21% Pro) were required for normal clock function (Figure 2C). The remainder of the C-terminus (amino acids 495 – 524, 28% Pro; 683 – 790, 24% Pro) contains a clock relevant region of PRD-2 based on deletion analyses. Further, PRD-2 SUZ domain and C-terminal deletion mutants are expressed at the protein level, indicating that clock defects must be due to the absent domain (Supplementary Figure 2A). PRD-2 is exclusively localized to the cytoplasm based on biochemical evaluation, and this localization does not change as a function of time of day (Figure 2D).

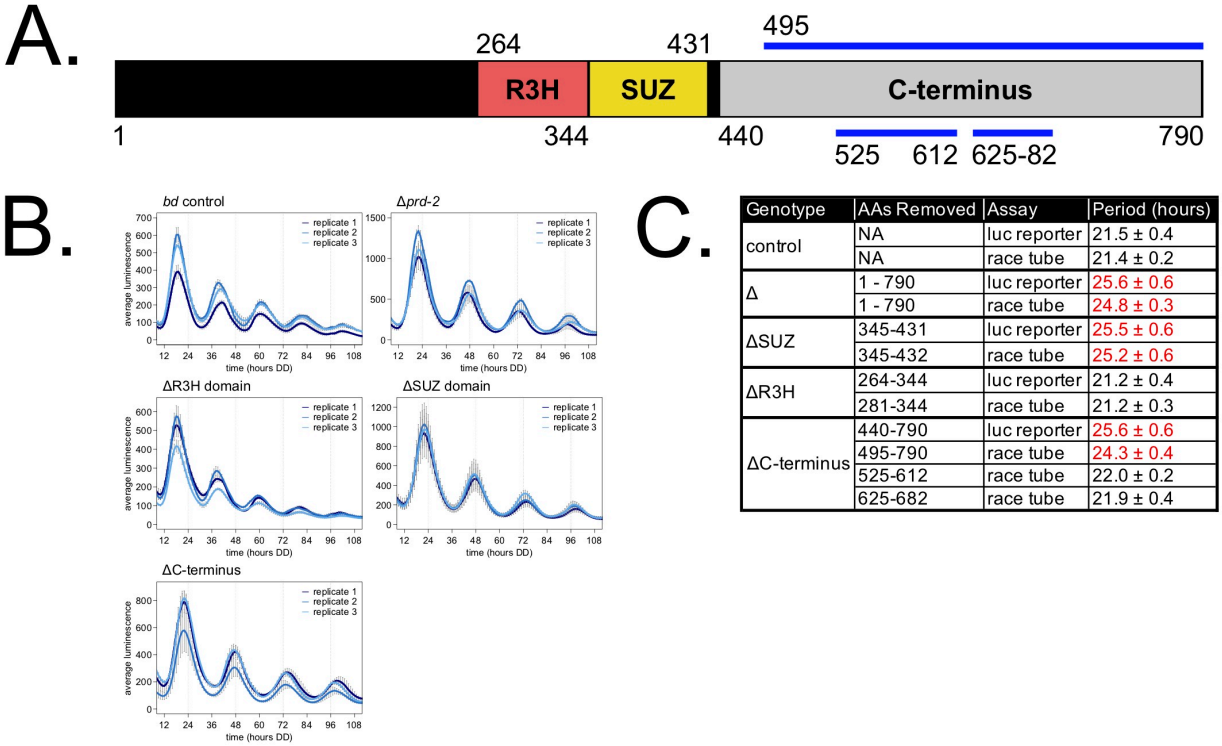

Figure 2. Clock-relevant protein domains and localization of PRD-2 suggest and RNA-binding function. PRD-2 has tandemly arrayed R3H and SUZ domains associated with RNA binding proteins, and its C-terminal region is highly enriched for proline (P) and glutamine (Q). The cartoon of PRD-2 protein lists relevant amino acid coordinates (**A**). The native NCU01019 locus was replaced with single domain deletion mutants, and 96-well plate luciferase assays were used to measure the circadian period length in triplicate wells per biological replicate experiment. A wild-type clock period was recovered in *ras-1*^{bd} controls and the *prd-2*ΔR3H mutant, while Δ*prd-2*, *prd-2*ΔSUZ, and *prd-2*ΔC-terminus had long period phenotypes (**B**). Independently constructed strains targeted domain deletion mutants to the *csr-1* locus in a Δ*prd-2* background (Supplementary Table 1), and mutant period lengths were determined by race tube assay. Period lengths (± 1 SD) show that the clock-relevant domains of PRD-2 are the

SUZ domain and the C-terminus (**C**). Total (T), Nuclear (N), and Cytosolic (C) fractions were prepared over a circadian time course (N = 1 per time point). γ-Tubulin (NCU03954) was used as a control for cytoplasmic localization and histone H3 (NCU01635) for nuclear localization. PRD-2 tagged with a C-terminal V5 epitope tag is localized to the cytoplasm throughout the circadian cycle (**D**).

NCU01019 RNA expression is not induced by light (Wu et al., 2014) nor rhythmically expressed over circadian time (Hurley et al., 2014). NCU01019 protein is abundant and shows weak rhythms (Hurley et al., 2018) (Supplementary Figure 2B), which suggests that PRD-2 oscillations are driven post-transcriptionally to peak in the early subjective morning, prior to the peak in the *frq* transcript (Aronson et al., 1994). Rhythms in PRD-2 protein expression were confirmed using a luciferase translational fusion (Supplementary Figure 2C), which peaked during the circadian day. *prd-2*^{INV} and ΔNCU01019 have a slight growth defect (Figure 1C) and are less fertile than wild-type as the female partner in a sexual cross (data not shown). Temperature and nutritional compensation of ΔNCU01019 alone are normal (Supplementary Figure 3), which was expected given the normal TC profile of the *prd-2*^{INV} mutant (Gardner and Feldman, 1981).

PRD-2 Regulates CKI Levels.

To identify the putative mRNA targets of PRD-2, we performed total RNA-Sequencing on triplicate samples of Δ*prd-2* versus control grown in constant light at 25°C. Hundreds of genes are affected by loss of PRD-2, but we did not identify a consensus functional category or sequence motif(s) for the putative PRD-2 regulon (Supplementary Figure 4). Given the pleotropic phenotypes of Δ*prd-2*, we posit that PRD-2 plays multiple roles in the cell, including regulation of carbohydrate and secondary metabolism. Focusing specifically on core clock genes, we found that *ck-1a*, *frq*, *wc-2*, *ckb-1* (regulatory beta subunit of CKII), and *frh* were significantly altered in the absence of PRD-2 (Figure 3A). Pursuing the top two hits, we found that the CKI transcript was dramatically less stable in Δ*prd-2* (Figure 3B), while *frq* mRNA stability was not significantly altered (Supplementary Figure 5). To demonstrate that PRD-2 binds the *ck-1a* transcript *in vivo*, we used RNA immunoprecipitation after UV crosslinking (CLIP). The Pumilio family RNA-binding protein PUF4 (NCU16560) was previously shown to bind in the 3' UTR of *cbp3* (NCU00057), *mrp-1* (NCU07386), and other target genes identified by HITS-CLIP high-throughput sequencing (Wilinski et al., 2017). C-terminally tagged alleles of

PRD-2, PUF4, and an untagged negative control strain were used to immunoprecipitate crosslinked RNAs (Materials & Methods). As expected, *cbp3* and *mrp-1* positive controls were significantly enriched in the PUF4 CLIP sample compared to the negative IP (Figure 3C). *ck-1a* is also enriched in the PRD-2 CLIP sample, demonstrating that the CKI transcript is a direct target of the PRD-2 protein (Figure 3C).

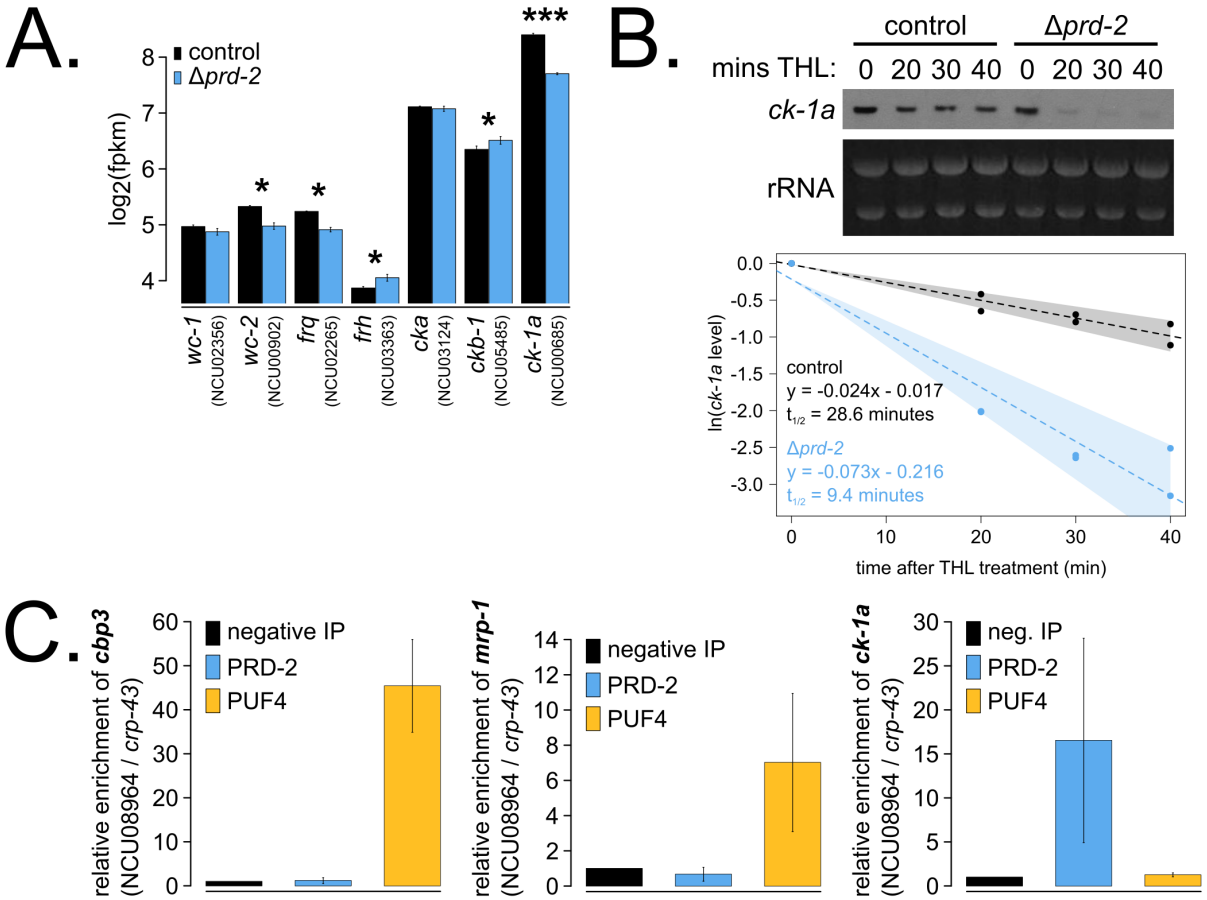

Figure 3. The core clock target of PRD-2 is the *casein kinase I* transcript. Control and Δ*prd-2* cultures were grown in the light at 25°C in Bird medium for 48 hours prior to RNA isolation. Expression levels for core clock genes were measured by RNA-Sequencing (N = 3 biological replicates per strain), and $\log_2$-transformed FPKM values are shown. Asterisks indicate $p < 0.05$ (*) or $p < 5x10^{-5}$ (***) by student's t-test compared to control levels. The *ck-1a* transcript is > 1.5x less abundant in Δ*prd-2* (**A**). *ck-1a* mRNA degradation kinetics were examined by Northern blot in a time course after treatment with thiolutin (THL) at approximately CT1 (N = 2 biological replicates). RNA levels were quantified using ImageJ, natural log transformed, fit with a linear model (`glm` in R, Gaussian family defaults), and half-life was calculated assuming first order

decay kinetics (ln(2) / slope). Shaded areas around the linear fit represent 95% confidence intervals on the slope. The *ck-1a* transcript is 3x less stable in Δ*prd-2* (**B**). The PUF4 (NCU16560) RNA-binding protein pulls down known target transcripts *cbp3* (NCU00057) and *mrp-1* (NCU07386) by RT-qPCR (N = 3 biological replicates). PRD-2 CLIP samples were processed in parallel with PUF4 positive controls, and PRD-2 binds the *ck-1a* transcript *in vivo* (**C**).

Hypothesizing that the clock-relevant target of PRD-2 could be CKI, we used two genetic approaches to manipulate CKI activity in an attempt to rescue the Δ*prd-2* long period phenotype. First, we placed the *ck-1a* gene under the control of the quinic acid inducible promoter (Mehra et al., 2009) and crossed this construct into the Δ*prd-2* background. We found that increasing expression of *ck-1a* using high levels (10^{-1} – 10^{-2} M) of QA partially rescued the Δ*prd-2* long period phenotype (Figure 4A). We also noticed a synergistic poor growth defect in the double mutant at 10^{-4} M QA, consistent with low levels of *ck-1a* (an essential gene in *Neurospora*: (Gorl et al., 2001; He et al., 2006)). There are two explanations for the lack of full rescue to periods shorter than 25 hours in the $P_{qa\text{-}2}$-*ck-1a* Δ*prd-2* double mutant: 1) even at saturating 10^{-1} M QA induction, the *qa-2* promoter may not reach endogenous levels of *ck-1a* achieved under its native promoter, and/or 2) because PRD-2 acts directly as an RNA-binding protein for CKI transcripts, simply increasing levels of *ck-1a* RNA cannot fully rescue PRD-2's role in stabilizing or positioning CKI transcripts in the cytoplasm.

Next, we turned to a previously described fungal CKI constitutively active allele, CKI $Q299^{STOP}$ (Querfurth et al., 2007), reasoning that we might be able to rescue low *ck-1a* levels in Δ*prd-2* by genetically increasing CKI kinase activity. We replaced endogenous CKI with a CKI^{SHORT} allele, which expresses only the shortest *ck-1a* isoform (361 amino acids). CKI^{SHORT} lacks 23 amino acids in the C-terminal tail of the full length isoform that are normally subject to autophosphorylation leading to kinase inhibition. This CKI^{SHORT} allele also carries an in-frame C-terminal HA3 tag and selectable marker, which displace the endogenous 3' UTR of *ck-1a*. The CKI^{SHORT} mutant has a short period phenotype (~17 hrs), presumably due to hyperactive kinase activity and rapid feedback loop closure (Liu et al., 2019). Significantly, the CKI^{SHORT} mutation is completely epistatic to Δ*prd-2* (Figure 4B), indicating that CKI is the clock-relevant target of PRD-2.

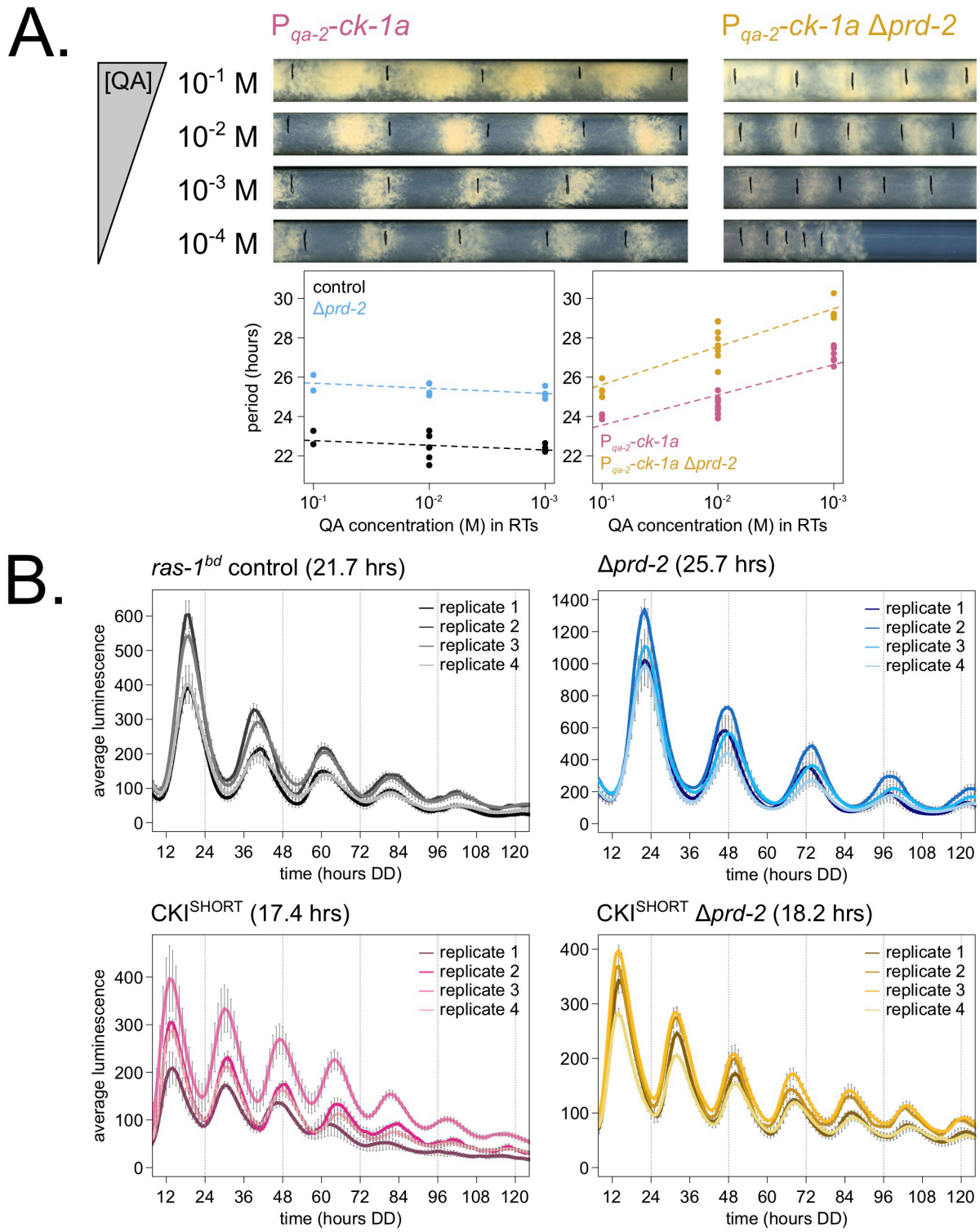

Figure 4. Genetically increasing CKI levels or activity rescues the Δ*prd-2* long period phenotype. Representative race tubes from *ras-1*^{bd} P$_{qa-2}$-*ck-1a* single (pink) and *ras-1*^{bd} P$_{qa-2}$-*ck-1a* Δ*prd-2* double (yellow) mutants are shown with growth using the indicated concentrations

of quinic acid (QA) to drive expression of *ck-1a*. All results are shown in a scatterplot, where each dot represents one race tube's free running period length. *ras-1^{bd}* controls (black) had an average period of 22.5 ± 0.5 hours (N = 12), and period length was not significantly affected by QA concentration (ANOVA p = 0.297). *ras-1^{bd}* Δ*prd-2* controls (blue) had an average period of 25.4 ± 0.4 hours (N = 10), and period length was not significantly affected by QA concentration (ANOVA p = 0.093). Period length of *ras-1^{bd} P$_{qa-2}$-ck-1a* single mutants (pink) was significantly altered across QA levels (ANOVA p = 3.6x10^{-6}), and the average period at 10^{-1} M QA was 24.3 ± 0.5 hours (N = 4). Period length of *ras-1^{bd}* P$_{qa-2}$*-ck-1a* Δ*prd-2* double mutants (yellow) was also significantly affected by QA levels (ANOVA p = 8.1x10^{-8}), and the average period at 10^{-1} M QA was 25.4 ± 0.4 hours (N = 4). The double mutant period length was not genetically additive at high levels of QA induction (**A**). A hyperactive CKI allele was constructed by expressing the shortest isoform only (CKI^{SHORT}). 96-well plate luciferase assays were used to measure the circadian period length. Traces represent the average of 3 technical replicates across 4 biological replicate experiments for: *ras-1^{bd}* controls (gray, $\tau = 21.7 \pm 0.3$ hours), *ras-1^{bd}* Δ*prd-2* (blue, $\tau = 25.7 \pm 0.6$ hours), *ras-1^{bd}* CKI^{SHORT} (pink, $\tau = 17.4 \pm 0.3$ hours), and *ras-1^{bd}* CKI^{SHORT} Δ*prd-2* double mutants (yellow, $\tau = 18.2 \pm 0.3$). CKI^{SHORT} is completely epistatic to Δ*prd-2* in double mutants (**B**).

Nonsense Mediated Decay Impacts the Clock by Regulating CKI Levels.

Nonsense Mediated Decay (NMD) in *Neurospora crassa* is triggered by two different types of RNA structures. Open reading frames in 5' UTRs that produce short peptides (5' uORFs) can trigger NMD in a mechanism that does not require the Exon Junction Complex (Zhang and Sachs, 2015). The *frq* transcript has 6 such uORFs (Colot et al., 2005; Diernfellner et al., 2005) and could be a bona fide NMD target because its splicing is disrupted in the absence of NMD (Wu et al., 2017). In addition, transcripts with long 3' UTRs, with intron(s) near a STOP codon, and/or with intron(s) in the 3' UTR, can also be degraded by NMD after recruitment of the UPF1/2/3 complex by the Exon Junction Complex in a pioneering round of translation (Zhang and Sachs, 2015).

Since the observation by Compton (Compton, 2003) that the short period mutant *period-6* identified the UPF1 core subunit of the NMD pathway, the clock-relevant target(s) of NMD has been an object of conjecture and active research. Because loss of NMD reduces the amount of the transcript encoding the short-FRQ protein isoform (Wu et al., 2017), and strains making only short-FRQ have slightly lengthened periods (Liu et al., 1997), Wu et al. (2017) recently speculated that the short period of the *period-6^{UPF1}* mutant might be explained by effects of

NMD on FRQ. However, strains expressing only long-FRQ display an essentially wild-type period length (Colot et al., 2005; Liu et al., 1997), not a short period phenotype like *prd-6*^{UPF1}; this finding is not consistent with FRQ being the only or even principal clock-relevant target of NMD, leaving unresolved the role of NMD in the clock.

To tackle this puzzle, we returned to classical genetic epistasis experiments and confirmed the observation that *prd-6* is completely epistatic to *prd-2*^{INV} (Morgan and Feldman, 2001), going on to show that in fact each of the individual NMD subunit knockouts, Δ*upf2* and Δ*upf3* as well as Δ*prd-6*^{upf1}, is epistatic to the Δ*prd-2* long period phenotype (Figure 5A). Previous work had profiled the transcriptome of Δ*prd-6* compared to a control (Wu et al., 2017); we re-processed this RNA-Seq data and found, exactly as in Δ*prd-2*, that *ck-1a* was the most affected core clock gene in Δ*prd-6* (Figure 5B). The *ck-1a* transcript has an intron located 70 nt away from its longest isoform's STOP codon, and its 3' UTR is, remarkably, among the 100 longest annotated UTRs in the entire *Neurospora* transcriptome (Figure 5C). Thus, *ck-1a* is a strong candidate for regulation by NMD.

We hypothesized that CKI is overexpressed in the absence of NMD (Figure 5B), leading to faster feedback loop closure and a short circadian period. To genetically control *ck-1a* levels, we crossed the regulatable P$_{qa\text{-}2}$-*ck-1a* allele into the Δ*prd-6* background and confirmed our hypothesis by finding that at low levels of inducer (10^{-5} M QA), decreased levels of *ck-1a* transcript revert the short period length of Δ*prd-6* to control period lengths (Figure 5D). Further, protein levels of CKI in the Δ*prd-6* background are reduced to control levels at 10^{-5} M QA (Figure 5E), which explains the period rescue phenotype. CKI protein is 2-3x more abundant in Δ*prd-6* and in Δ*prd-2* Δ*prd-6* (Figure 5F), matching its overexpression in the Δ*prd-6* transcriptome (Figure 5B). CKI protein is 3x reduced in Δ*prd-2* (Figure 5F), also correlating with its reduced mRNA expression and stability (Figure 3). We conclude that CKI is also the clock-relevant target of PRD-6^{UPF1}, placing NMD, PRD-2, and CKI in the same genetic epistasis pathway.

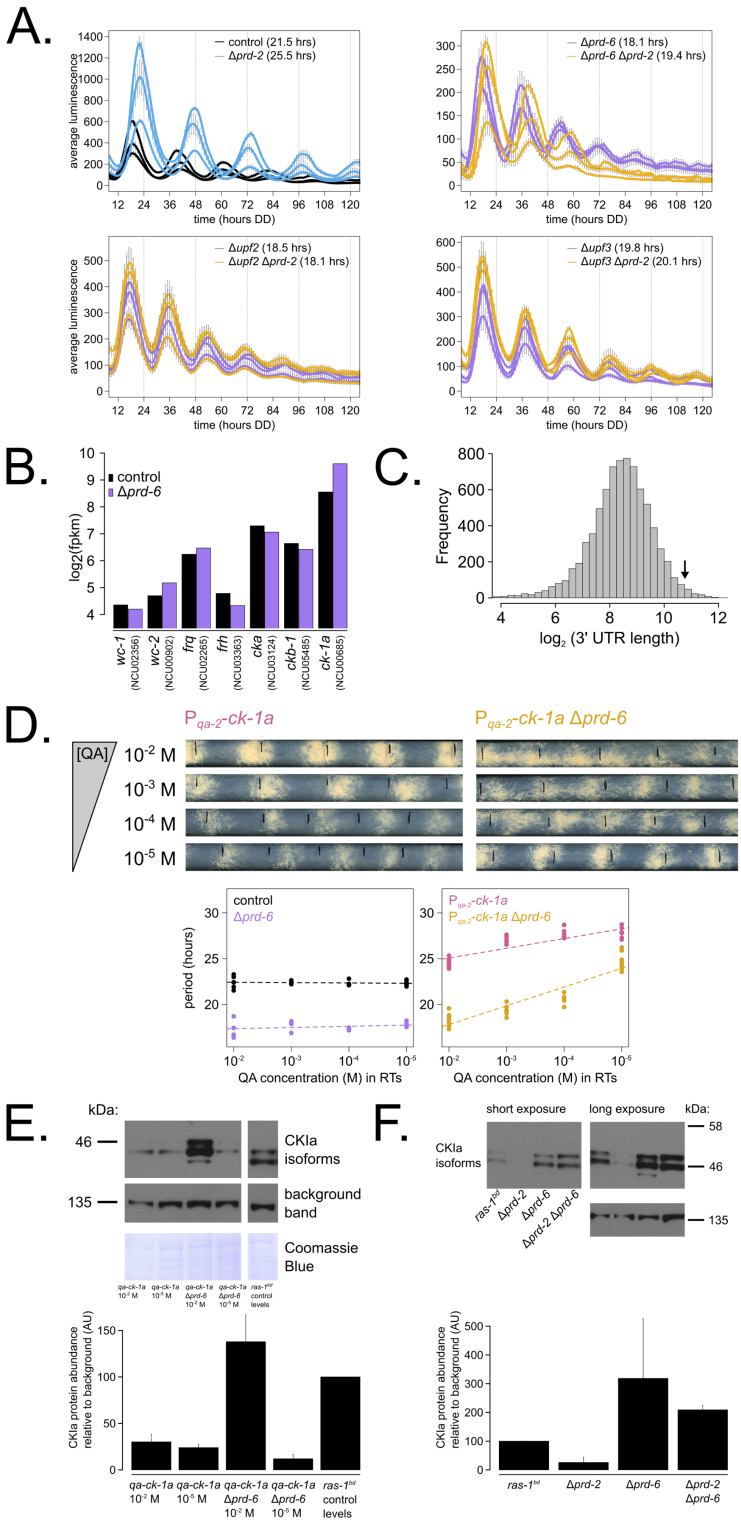

Figure 5. Nonsense Mediated Decay negatively regulates CKI levels via PRD-6, establishing a basis for the *prd-6 prd-2* genetic epistasis on circadian period length. 96-well plate luciferase assays were used to measure the circadian period length in triplicate wells

per three biological replicate experiments for: *ras-1*^{bd} controls (black, $\tau = 21.5 \pm 0.3$ hours), *ras-1*^{bd} Δ*prd-2* (blue, $\tau = 25.5 \pm 0.4$ hours); *ras-1*^{bd} Δ*prd-6* (purple, $\tau = 18.1 \pm 0.2$ hours), *ras-1*^{bd} Δ*prd-6* Δ*prd-2* double mutants (yellow, $\tau = 19.4 \pm 0.7$ hours); *ras-1*^{bd} Δ*upf2* (purple, $\tau = 18.5 \pm 0.5$ hours), *ras-1*^{bd} Δ*upf2* Δ*prd-2* double mutants (yellow, $\tau = 18.1 \pm 0.3$ hours); *ras-1*^{bd} Δ*upf3* (purple, $\tau = 19.8 \pm 0.3$ hours), *ras-1*^{bd} Δ*upf3* Δ*prd-2* double mutants (yellow, $\tau = 20.1 \pm 0.2$ hours). Each individual NMD subunit knockout is epistatic to the Δ*prd-2* long period phenotype (**A**). Raw RNA-Seq data from a previous study (Wu et al., 2017) were analyzed using the same pipeline as data from Figure 3A (see Materials & Methods). Control and Δ*prd-6* gene expression levels (log_2-transformed) are shown for core clock genes. The *ck-1a* transcript is > 2x more abundant in Δ*prd-6* (**B**). 3' UTR lengths from 7,793 genes were mined from the *N. crassa* OR74A genome annotation (FungiDB version 45, accessed on 10/25/2019), and plotted as a histogram. The arrow marks the 3' UTR of *ck-1a*, which is 1,739 bp and within the top 100 longest annotated UTRs in the entire genome (**C**). Representative race tubes from *ras-1*^{bd} P_{qa-2}-*ck-1a* single (pink) and *ras-1*^{bd} P_{qa-2}-*ck-1a* Δ*prd-6* double (yellow) mutants are shown at the indicated concentrations of quinic acid to drive expression of *ck-1a*. All results are shown in a scatterplot, where each dot represents one race tube's free running period length. *ras-1*^{bd} controls (black) had an average period of 22.4 ± 0.4 hours (N = 20), and period length was not significantly affected by QA concentration (ANOVA p = 0.605). *ras-1*^{bd} Δ*prd-6* controls (purple) had an average period of 17.5 ± 0.6 hours (N = 16), and period length was not significantly affected by QA concentration (ANOVA p = 0.362). Period length of *ras-1*^{bd} P_{qa-2}-*ck-1a* single mutants (pink) was significantly altered across QA levels (ANOVA $p = 2.9 \times 10^{-8}$), and the average period at 10^{-5} M QA was 27.6 ± 0.8 hours (N = 8). Period length of *ras-1*^{bd} P_{qa-2}-*ck-1a* Δ*prd-6* double mutants (yellow) was also significantly affected by QA levels (ANOVA $p = 9.4 \times 10^{-12}$), and the average period at 10^{-5} M QA was 24.7 ± 0.9 hours (N = 8). Thus, the double mutant period length was not genetically additive at low levels of QA induction, and the short period phenotype of Δ*prd-6* is rescued (**D**). CKI protein levels were measured from the indicated genotypes grown in 0.1% glucose LCM medium with QA supplemented at the indicated concentrations for 48 hours in constant light. A representative immunoblot of 3 biological replicates is shown, and replicates are quantified in the bar graph relative to *ras-1*^{bd} control CKI levels from a 2% glucose LCM culture (**E**). CKI protein levels were measured from the indicated genotypes grown in 2% glucose LCM medium for 48 hours in constant light. A representative immunoblot of 3 biological replicates is shown, and replicates are quantified in the bar graph relative to *ras-1*^{bd} control CKI levels (**F**). CKI protein levels are increased in Δ*prd-6*, decreased in

the Δ*prd-2* mutant, and Δ*prd-6* is epistatic to Δ*prd-2* with respect to CKI levels and circadian period length.

Discussion

By uncovering the identity and mode of action of PRD-2 and exploring the mechanism of two classical *period* mutants, *prd-2* and *prd-6*, we found a common basis in regulation of CKI levels, which are under tight control in the *Neurospora* clock (Figure 6). That the mechanistic basis of action of two independently derived non-targeted clock mutants centers on regulation of the activity of a single enzyme, CKI, via two distinct mechanisms is noteworthy. Period-2 encodes an RNA-binding protein (Figures 1-2) that stabilizes the CKI transcript (Figure 3B). We demonstrate that CKI is the most important core clock target of PRD-2 by rescuing its long period mutant phenotype with a hyperactive CKI allele (Figure 4B). The predominantly cytoplasmic localization of PRD-2 (Figure 2D) is consistent with its action in protecting *ck-1a* transcripts from NMD and rounds out the model. PTBP1, an RNA-binding protein, protects its target transcripts from NMD-mediated degradation by binding in the 3' UTR and blocking NMD recruitment in mouse (Ge et al., 2016), and future work will determine if PRD-2 functions similarly to PTBP1.

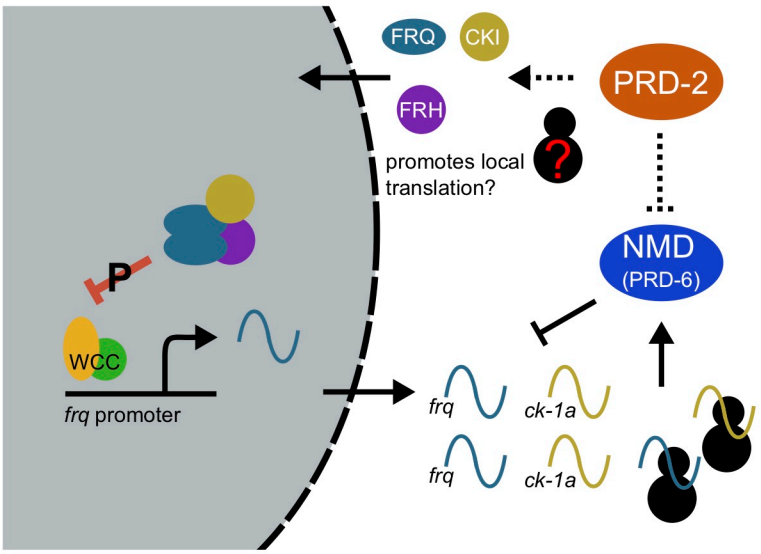

Figure 6. Counter balancing regulation of CKI provides a unifying genetic model for the action of PRD-2 and PRD-6^{UPF-1} in the circadian oscillator. The NMD complex (PRD-6^{UPF1}, UPF2, and UPF3) targets the *frq* and *ck-1a* transcripts for degradation after the first round of translation (upstream uORFs in *frq*; long 3' UTR in *ck-1a*). PRD-2 binds to and stabilizes *ck-1a*

transcripts (dashed lines), which could also promote local translation and complex formation for the negative arm of the clock. In the absence of PRD-2, the long period phenotype is due to low CKI levels, and in the absence of NMD, the short period phenotype is due to high CKI levels.

PRD-6 and the NMD machinery target *ck-1a* mRNA for degradation to regulate its expression levels, presumably mediated by the long 3' UTR of *ck-1a* transcripts in *Neurospora* (Figure 5). NMD components are not rhythmic in abundance in the fungal clock (Hurley et al., 2014, 2018). These data, taken together with the constitutive expression of the CKI mRNA and protein (Baker et al., 2009; Gorl et al., 2001; Hurley et al., 2014, 2018), lead us to predict that NMD regulation of CKI occurs throughout the circadian cycle. To our knowledge the discovery of NMD regulation of CKI represents a wholly novel and potentially important mode of regulation for this pivotal kinase. Future work will investigate whether insect DBT and/or mammalian CKIδ/ε (CSNK1D, CSNK1E) are also targets of NMD. Long UTR length appears to be conserved across CKI orthologs (Supplementary Figure 6). One previous study in *Drosophila* reported a circadian period defect in a tissue-specific NMD knockdown (Ri et al., 2019), but the behavioral rhythm was lengthened in UPF1-depleted insects unlike the short period defect observed in *Neurospora*. In mouse, both CKIε and CLOCK display altered splicing patterns in the absence of UPF2 (Weischenfeldt et al., 2012). Most core clock proteins have at least one uORF in mammals (Millius and Ueda, 2017), altogether raising the possibility that multiple core clock genes are regulated by NMD. The importance of NMD has already been recognized and investigated in the plant clock, where alternative splicing leads to NMD turnover for 4 core clock and accessory mRNAs: GRP7, GRP8, TOC1, and ELF3 (reviewed in: (Mateos et al., 2018)).

CKI abundance and alternative isoforms strongly affect circadian period length. Low levels of CKI driven from an inducible promoter lead to long periods approaching 30 hours (Mehra et al., 2009) (Figure 4A). In the mammalian clock, decreased CKI expression also significantly lengthens period (Isojima et al., 2009; Lee et al., 2009; Tsuchiya et al., 2016). CKI is rendered hyperactive by removing its conserved C-terminal domain, a domain normally subject to autophosphorylation leading to kinase inhibition (Guo et al., 2019; Querfurth et al., 2007). We generated a CKI mutant expressing only this shortest CKI isoform, finding a 17.5 hour short period phenotype in the absence of C-terminal autophosphorylation (Figure 4B). Based on prior work, increased CKI activity and/or abundance would be expected to increase FRQ-CKI affinity and lead to faster feedback loop closure (Liu et al., 2019), consistent with the short period phenotype. Curiously, this CKI short isoform is expressed at levels similar to the full

length isoform in *Neurospora* (as well as a third short isoform derived from an alternative splice acceptor event) (Figure 5F), and all isoforms interact with FRQ by immunoprecipitation (Querfurth et al., 2007). Why do natural isoforms arise without the auto-inhibitory C-terminus in *Neurospora*, and are these regulatory events required to keep the clock on time? Mammalian alternative isoforms *CKIδ1 and CKIδ2* have different substrate preferences *in vitro*, which leads to differential phosphorylation of PER2 whereby CKIδ2 phosphorylation significantly stabilizes PER2 (Fustin et al., 2018). Adding further complexity, *CKIδ1 and CKIδ2* isoform expression patterns appear to be tissue specific and are regulated by m6A RNA modification. Regulation of CKI levels and isoform expression is an important direction for future work in the circadian clock.

Casein Kinase I has a diverse array of functions in eukaryotes and is critically important in human health (reviewed in: (Cheong and Virshup, 2011; Vielhaber and Virshup, 2001)). CKI overexpression is pathogenic in Alzheimer's Disease in addition to its role in circadian period regulation (Sundaram et al., 2019). Future work on regulation of CKI levels and isoform expression will shed light on CKI regulation in the clock, in development, and in disease.

Materials and Methods

Neurospora strains and growth conditions.

The *ras-1^{bd} prd-2^{INV}* strains 613-102 (*mat* A) and 613-43 (*mat* a) were originally isolated in the Feldman laboratory (Lewis, 1995). Strains used in this study were derived from the wild-type background (FGSC2489 *mat* A), *ras-1^{bd}* background (87-3 *mat* a or 328-4 *mat* A), Δ*mus-51* background (FGSC9718 *mat* a), or the Fungal Genetics Stock Center (FGSC) knockout collection as indicated (Supplementary Table 1). Strains were constructed by transformation or by sexual crosses using standard *Neurospora* methods (http://www.fgsc.net/Neurospora/NeurosporaProtocolGuide.htm). In the "c box-luc" core clock transcriptional reporter used throughout, a codon-optimized firefly luciferase gene is driven by the clock box in the *frequency* promoter (Gooch et al., 2008; Hurley et al., 2014; Larrondo et al., 2015). The clock reporter construct was targeted to the *csr-1* locus and selected on resistance to 5 μg/ml cyclosporine A (Sigma # 30024) (Bardiya and Shiu, 2007).

Standard race tube (RT) medium was used for all race tubes (1X Vogel's Salts, 0.1% glucose, 0.17% arginine, 1.5% agar, and 50 ng/ml biotin). Where indicated, D-Quinic Acid (Sigma # 138622) was added from a fresh 1 M stock solution (pH 5.8). Standard 96-well plate medium was used for all camera runs (1X Vogel's Salts, 0.03% glucose, 0.05% arginine, 1.5% agar, 50 ng/ml biotin, and 25 μM luciferin from GoldBio # 115144-35-9). Liquid cultures were

started from fungal plugs as described (Chen et al., 2009; Nakashima, 1981) or from a conidial suspension at $1x10^5$ conidia/ml. Liquid cultures were grown in 2% glucose Liquid Culture Medium (LCM) or in 1.8% glucose Bird Medium (Metzenberg, 2004) as indicated. QA induction experiments in liquid culture were performed in 0.1% glucose LCM medium with QA supplemented. All experiments were conducted at 25°C in constant light unless otherwise indicated.

Strains were genotyped by screening for growth on selection medium (5 µg/ml cyclosporine A, 400 µg/ml Ignite, and/or 200-300 µg/ml Hygromycin). PCR genotyping was performed on gDNA extracts from conidia incubated with Allele-In-One Mouse Tail Direct Lysis Buffer (Allele Biotechnology # ABP-PP-MT01500) according to the manufacturer's instructions. GreenTaq PCR Master Mix (ThermoFisher # K1082) was used for genotyping. Relevant genotyping primers for key strains are:

ras-1^{bd} (mutant): 5' TGCGCGAGCAGTACATGCGAAT and 5' CCTGATTTCGCGGACGAGATCGTA 3'

ras-1^{WT} (NCU08823): 5' GCGCGAGCAGTACATGCGGAC 3' and 5' CCTGATTTCGCGGACGAGATCGTA 3'

prd-2^{WT} (NCU01019): 5' CACTTCCAGTTATCTCGTCAC 3' and 5' CACAACCTTGTTAGGCATCG 3'

Δ*prd-2*::bar^{R} (KO mutant): 5' CACTTCCAGTTATCTCGTCAC 3' and 5' GTGCTTGTCTCGATGTAGTG 3'

prd-2^{INV} (left breakpoint): 5' AGCGAGCTGATATGCCTTGT 3' and 5' CGACTTCCACCACTTCCAGT 3'

prd-2^{INV} (right breakpoint): 5' TGTTTGTCCGGTGAAGATCA 3' and 5' GTCGTGGAATGGGAAGACAT 3'

Δ*prd-6*::hyg^{R} (FGSC KO mutant): 5' CTGCAACCTCGGCCTCCT 3' and 5' CAGGCTCTCGATGAGCTGATG 3'

bar^{R}::P$_{qa\text{-}2}$-*ck-1a* (QA inducible CKI): 5' GTGCTTGTCTCGATGTAGTG 3' and 5' GATGTCGCGGTGGATGAACG 3'

RNA stability assays.

Control and Δ*prd-2* liquid cultures grown in 1.8% glucose Bird medium were age-matched and circadian time (CT) matched to ensure that RNA stability was examined at the same phase of the clock. Control cultures were shifted to constant dark for 12 hours, and Δ*prd-2* cultures were shifted to dark for 14 hours (~CT1 for 22.5-hour wild-type period and for 26-hour

534 Δ*prd-2* period; 46 hours total growth). Thiolutin (THL; Cayman Chemical # 11350) was then
535 added to a final concentration of 12 μg/ml to inhibit new RNA synthesis. Samples were collected
536 every 10 minutes after THL treatment by vacuum filtration and flash frozen in liquid nitrogen.
537 THL has multiple off-target effects in addition to inhibiting transcription (Lauinger et al., 2017).
538 For this reason, *frq* mRNA degradation kinetics were also examined with an alternative protocol.
539 Light-grown, age-matched liquid Bird cultures of wild-type and Δ*prd-2* were shifted into the dark
540 and sampled every 10 minutes to measure *frq* turnover; transcription of *frq* ceases immediately
541 on transfer to darkness (Heintzen et al., 2001; Tan et al., 2004). All tissue manipulation in the
542 dark was performed under dim red lights, which do not reset the *Neurospora* clock (Chen et al.,
543 2009).
544
545 **RNA isolation and detection.**
546 Frozen *Neurospora* tissue was ground in liquid nitrogen with a mortar and pestle. Total
547 RNA was extracted with TRIzol (Invitrogen # 15596026) and processed as described (Chen et
548 al., 2009). RNA samples were prepared for RT-qPCR, Northern Blotting, RNA-Sequencing, or
549 stored at -80°C.
550 For RT-qPCR, cDNA was synthesized using the SuperScript III First-Strand synthesis kit
551 (Invitrogen # 18080-051). RT-qPCR was performed using SYBR green master mix (Qiagen #
552 204054) and a StepOne Plus Real-Time PCR System (Applied Biosystems). C_t values were
553 determined using StepOne software (Life Technologies) and normalized to the *actin* gene (ΔC_t).
554 The $\Delta\Delta C_t$ method was used to determine mRNA levels relative to a reference time point.
555 Relevant RT-qPCR primer sequences are: *prd-2* (NCU01019): 5'
556 GGGCAACGACGTCAAACTAT 3' and 5' TGCGTGTACATCACTCTGGA 3'. *actin* (NCU04173):
557 5' GGCCGTGATCTTACCGACTA 3' and 5' TCTCCTTGATGTCACGAACG 3'.
558 Northern probes were first synthesized using the PCR DIG Probe Synthesis Kit (Roche #
559 11 636 090 910). The 512 bp *frq* probe was amplified from wild-type *Neurospora* genomic DNA
560 with primers: 5' CTCTGCCTCCTCGCAGTCA 3' and 5'
561 CGAGGATGAGACGTCCTCCATCGAAC 3'. The 518 bp *ck-1a* probe was amplified with
562 primers: 5' CCATGCCAAGTCGTTCATCC 3' and 5' CGGTCCAGTCAAAGACGTAGTC 3'. Total
563 RNA samples were prepared according to the NorthernMax™-Gly Kit instructions (Invitrogen #
564 AM1946). Equal amounts of total RNA (5 – 10 μg) were loaded per lane of a 0.8 – 1% w/v
565 agarose gel. rRNA bands were visualized prior to transfer to validate RNA integrity. Transfer
566 was completed as described in the NorthernMax™-Gly instructions onto a nucleic acid
567 Amersham Hybond-N+ membrane (GE # RPN303B). Transferred RNA was crosslinked to the

membrane using a Stratalinker UV Crosslinker. The membrane was blocked and then incubated overnight at 42°C in hybridization buffer plus the corresponding DIG probe. After washing with NorthernMax™-Gly Kit reagents, subsequent washes were performed using the DIG Wash and Block Buffer Set (Roche # 11 585 762 001). Anti-Digoxigenin-AP Fab fragments were used at 1:10,000. Chemiluminescent detection of anti-DIG was performed using CDP-Star reagents from the DIG Northern Starter Kit (Roche # 12 039 672 910). Densitometry was performed in ImageJ.

Total RNA was submitted to Novogene for stranded polyA+ library preparation and sequencing. 150 bp paired-end (PE) read libraries were prepared, multiplexed, and sequenced in accordance with standard Illumina HiSeq protocols. 24.8 ± 1.7 million reads were obtained for each sample. Raw FASTQ files were aligned to the *Neurospora crassa* OR74A NC12 genome (accessed September 28, 2017 via the Broad Institute: ftp://ftp.broadinstitute.org/pub/annotation/fungi/neurospora_crassa/assembly/) using STAR (Dobin et al., 2013). On average, 97.6 ± 0.3% of the reads mapped uniquely to the NC12 genome. Aligned reads were assembled into transcripts, quantified, and normalized using Cufflinks2 (Trapnell et al., 2013). Triplicate control and Δ*prd-2* samples were normalized together with CuffNorm, and the resulting FPKM output was used in the analyses presented. RNA-Sequencing data have been submitted to the NCBI Gene Expression Omnibus (GEO; https://www.ncbi.nlm.nih.gov/geo/) under accession number GSE155999.

CLIP assay.

CLIP was performed using PUF4 (NCU16560) as a positive control RNA-binding protein from (Wilinski et al., 2017), with modifications. *Neurospora* strains containing endogenous locus C-terminally VHF tagged PUF4, PRD-2, or untagged negative control were used (Supplementary Table 1). Liquid cultures were grown in 2% glucose LCM for 48 hours in constant light. Tissue was harvested by vacuum filtration and fixed by UV crosslinking for 7 minutes on each side of the fungal mat (Stratalinker UV Crosslinker 1800 with 254-nm wavelength bulbs). UV crosslinked tissue was frozen in liquid nitrogen and ground into a fine powder with a mortar and pestle. Total protein was extracted in buffer (25 mM Tris-HCl pH 7.4, 150 mM NaCl, 2 mM $MgCl_2$, 0.5% NP-40, 1 mM DTT, 1x cOmplete protease inhibitor, 100 U / ml RNAse Out) and concentration determined by Bradford Assay. Approximately 10 mg of total protein was added to 30 µl anti-FLAG M2 magnetic beads (Sigma # M8823) prepared according to the manufacturer's instructions. Beads and lysate were rotated for 4 hours at 4°C, followed by 4 washes in 750 µl extraction buffer. Bound RNA-binding proteins were eluted with 100 µl 0.1 M

glycine-HCl pH 3.0 for 10 minutes. The supernatant was collected using a magnetic rack (NEB S1506S) and neutralized in 10 µl of 1 M Tris pH 8.0. The elution was incubated with 300 µl of TRIzol (Invitrogen # 15596026) for 10 minutes to extract RNA. Total RNA was isolated, DNAse treated, and concentrated using the Direct-zol RNA Microprep Kit (Zymo # R2062) following the manufacturer's instructions.

Equal amounts of immunoprecipitated RNA (~ 50 ng) were converted into cDNA using the oligo(dT) method from the SuperScript IV First-Strand synthesis kit (Invitrogen # 18091-050). RT-qPCR was performed using SYBR green master mix (Qiagen # 204054) and a StepOne Plus Real-Time PCR System (Applied Biosystems). C_t values were determined using StepOne software (Life Technologies) and normalized to the *crp-43* gene (ΔC_t) instead of the *actin* (NCU04173) gene because *actin* is a putative PUF4 target by HITS-CLIP (Wilinski et al., 2017). The $\Delta\Delta C_t$ method was used to determine target mRNA enrichment relative to the negative IP sample. Relevant RT-qPCR primer sequences were designed to flank introns: *cbp3* (NCU00057; PUF4 target): 5' CGAGAAATTCGGCCTTCTCCC 3' and 5' GCCTGGTGGAAGAAGTGGT 3'. *mrp-1* (NCU07386; PUF4 target): 5' TAGTAGGCACCGACTTTGAGCA 3' and 5' CGGGGACAGGTGGTCGAA 3'. *ck-1a* (NCU00685; PRD-2 target): 5' CGCAAACATGACTACCATG 3' and 5' CTCTCCAGCTTGATGGCA 3'. *crp-43* (NCU08964; normalization control): 5' CTGTCCGTACTCGTGACTCC 3' and 5' ACCATCGATGAGGAGCTTGC 3'.

Protein isolation and detection.

Frozen *Neurospora* tissue was ground in liquid nitrogen with a mortar and pestle. Total protein was extracted in buffer (50 mM HEPES pH 7.4, 137 mM NaCl, 10% glycerol v/v, 0.4% NP-40 v/v, and cOmplete Protease Inhibitor Tablet according to instructions for Roche # 11 836 170 001) and processed as described (Garceau et al., 1997). Protein concentrations were determined by Bradford Assay (Bio-Rad # 500-0006). For Western blots, equal amounts of total protein (10 - 30 µg) were loaded per lane into 4-12% Bis-Tris Bolt gels (Invitrogen # NW04125BOX). Western transfer was performed using an Invitrogen iBlot system (# IB21001) and PVDF transfer stack (# IB401001). Primary antibodies used for Western blotting were anti-V5 (1:3000, ThermoFisher # R960-25), anti-Tubulin alpha (1:10,000, Fitzgerald # 10R-T130a), or anti-CK1a (1:1000, rabbit raised). The secondary antibodies, goat anti-mouse or goat anti-rabbit HRP, were used at 1:5000 (Bio-Rad # 170-6516, # 170-6515). SuperSignal West Pico PLUS Chemiluminescent Substrate (ThermoFisher # 34578) or Femto Maximum Sensitivity

Substrate (Thermo # 34095) was used for detection. Immunoblot quantification and normalization were performed in ImageJ.

Nuclear and cytosolic fractions were prepared as previously described (Hong et al., 2008). Approximately 10 μg of total protein from each fraction were loaded for immunoblotting. Primary antibodies for fraction controls were histone H3A (Fitzgerald) and γ-tubulin (Abcam). HRP-conjugated secondary antibodies (Bio-Rad) were used with SuperSignal West Pico ECL (Thermo) for detection.

Luciferase reporter detection and data analysis.

96-well plates were inoculated with conidial suspensions from strains of interest and entrained in 12 hour light:dark cycles for 2 days in a Percival incubator at 25°C. Temperature inside the Percival incubator was monitored using a HOBO logger device (Onset # MX2202) during entrainment and free run. Plates were then transferred into constant darkness to initiate the circadian free run. Luminescence was recorded using a Pixis 1024B CCD camera (Princeton Instruments). Light signal was acquired for 10 – 15 minutes every hour using LightField software (Princeton Instruments, 64-bit version 6.10.1). The average intensity of each well was determined using a custom ImageJ Macro (Larrondo et al., 2015), and background correction was performed for each frame. Results from two different algorithms were averaged together to determine circadian period from background-corrected luminescence traces. The MESA algorithm was used as previously described (Kelliher et al., 2020). A second period measurement was obtained from an ordinary least squares autoregressive model to compute the spectral density (in R: `spec.ar(…, method = "ols")`). Race tube period lengths were measured from scans using ChronOSX 2.1 software (Roenneberg and Taylor, 2000).

Data visualization.

All figures were plotted in R, output as scalable vector graphics, formatted using Inkscape, and archived in R markdown format. Data represent the mean of at least three biological replicates with standard deviation error bars, unless otherwise indicated.

669 **Supplementary Figures**

670

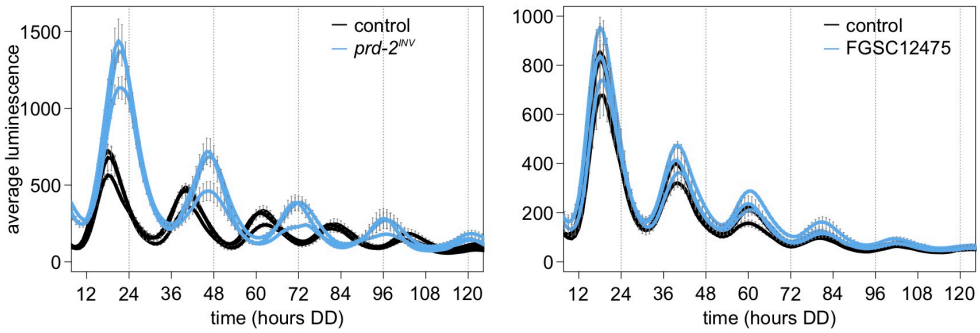

671

672 **Supplementary Figure 1. NCU03775 knockout has a normal circadian period and does**
673 **not explain the *prd-2*^{INV} phenotype.** 96-well plate luciferase assays were used to measure the
674 circadian period length. Traces represent the average of 3 technical replicates across 3
675 biological replicate experiments for: *ras-1*^{bd} controls (black, $\tau = 21.9 \pm 0.3$ hours), *ras-1*^{bd} *prd-2*^{INV}
676 (blue, $\tau = 25.6 \pm 0.4$ hours), wild-type controls (black, $\tau = 21.7 \pm 0.3$ hours), and the knockout
677 strain FGSC12475 (blue, $\tau = 21.7 \pm 0.3$ hours). ΔNCU03775 has a wild-type circadian period
678 length.

679

680

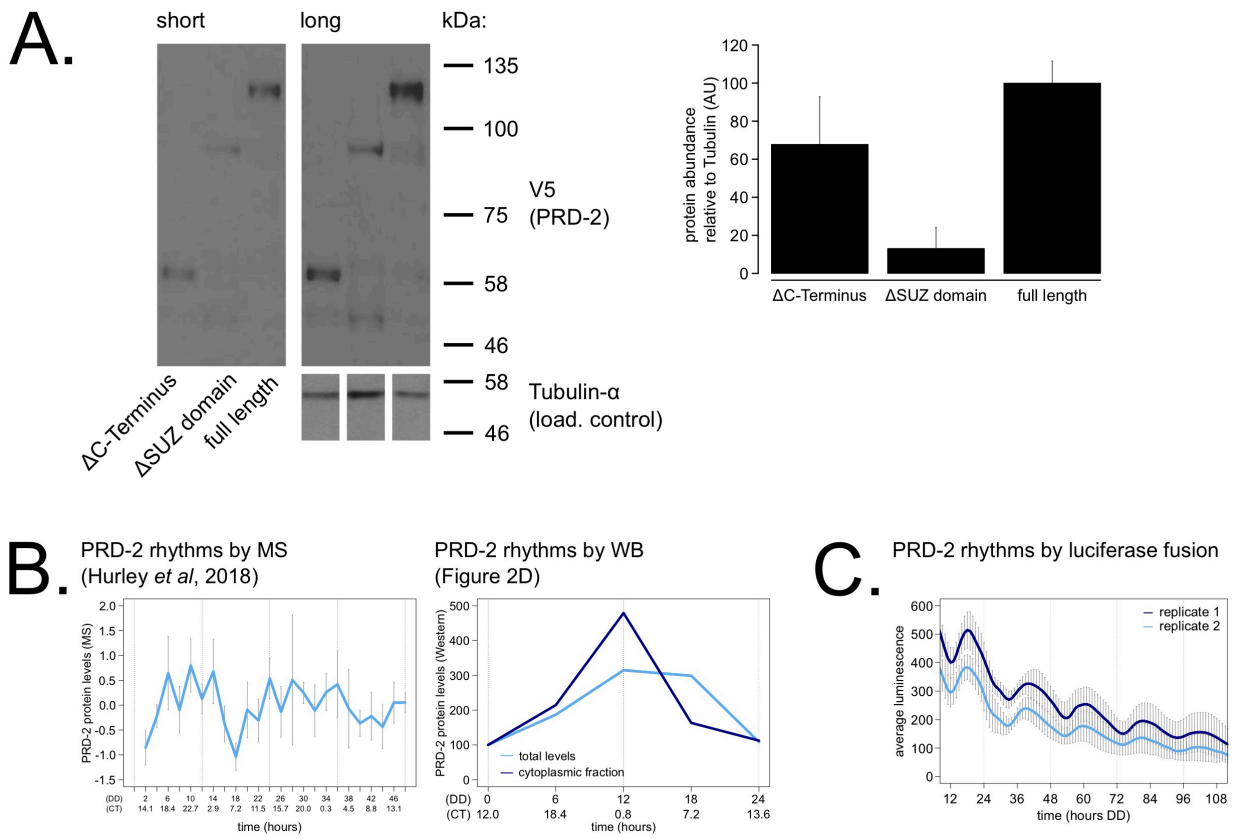

Supplementary Figure 2. PRD-2 protein levels are slightly rhythmic and are detectable in protein domain deletion mutants. PRD-2 protein levels were measured from at least 3 biological replicates using strains where the endogenous NCU01019 locus was replaced with V5-tagged domain deletion constructs: *prd-2*ΔC-Terminus(Δ440-790), *prd-2*ΔSUZ(Δ345-431), and full length. Long and short exposures of a representative immunoblot are shown with quantification relative to tubulin loading controls (**A**). The C-Terminal deletion strain has ~68% PRD-2 levels compared to the full length control, and the SUZ deletion has ~13% levels. Both are above the low levels of *qa*-driven NCU01019 needed to induce the long period phenotype (Figure 1E). MS data from a previous study (Hurley et al., 2018) revealed low amplitude rhythms in PRD-2 abundance with a broad peak in the subjective circadian night and early morning (~ CT18 – 2). Circadian Time (CT) was calculated as described previously (Kelliher et al., 2020). PRD-2 abundance was also quantified from the localization time course (Figure 2D) relative to tubulin and relative to the first time point. Peak PRD-2 protein abundance was observed in the subjective morning from both MS and immunoblot data (**B**), corresponding with the rise in *frq* transcript levels (Aronson et al., 1994). To confirm rhythms in PRD-2 protein expression, the complete NCU01019 5' UTR and coding sequence, plus 951 bp of upstream promoter sequence, was fused in-frame with codon-optimized luciferase (Gooch et al., 2008), not

699 including its endogenous 3' UTR sequence. This construct was transformed into the *prd-2*^{WT}
700 background at the *csr-1* locus, and PRD-2 protein cycles in abundance (τ = 21.7 ± 0.8 hours).
701 PRD-2 protein peaks during the circadian day (CT7.5 ± 1) by luciferase fusion (**C**), slightly
702 delayed relative to its morning peak by Western and MS.
703
704

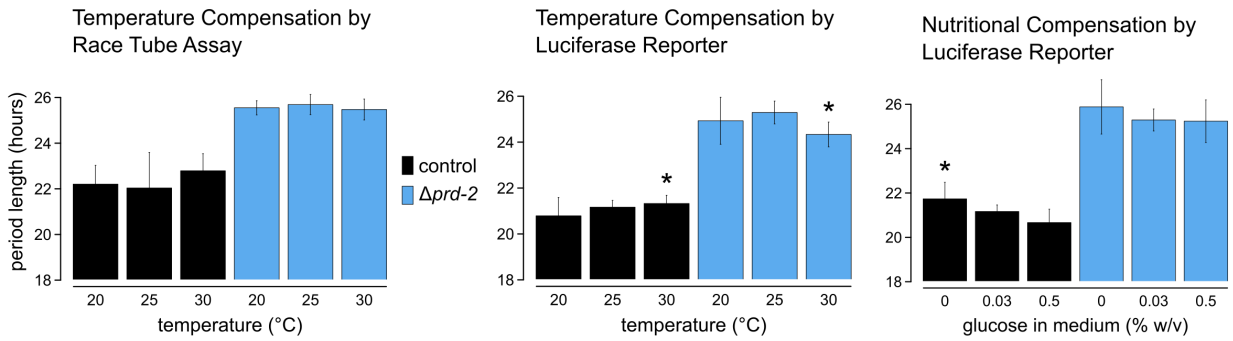

705
706 **Supplementary Figure 3. Temperature and nutritional compensation are normal in**
707 **ΔNCU01019.** Temperature and nutritional compensation were assessed in *ras-1*^{bd} controls
708 compared to *ras-1*^{bd} Δ*prd-2*. Race tubes were incubated at 20°, 25°, or 30°C to determine free
709 running period length. Temperature did not significantly affect period length for controls (ANOVA
710 p = 0.598) or for the Δ*prd-2* mutant (ANOVA p = 0.756) race tubes. 96-well plates were
711 incubated at 20°, 25°, or 30°C to determine free running period length. Period was significantly
712 different at 30°C for both genotypes (Asterisks (*): control 20°C vs 30°C, Tukey Test p = 0.023;
713 Δ*prd-2* 20°C vs 30°C, Tukey Test p = 0.037; Δ*prd-2* 25°C vs 30°C, Tukey Test p = 0.0002). 96-
714 well plates were run with 0%, 0.03%, or 0.5% glucose w/v to test nutritional compensation.
715 Period length was significantly different at 0% glucose for controls only (Asterisk (*): control 0%
716 vs 0.5%, Tukey Test p = 0.00005; control 0% vs 0.03%, Tukey Test p = 0.034; Δ*prd-2* ANOVA p
717 = 0.183).
718
719

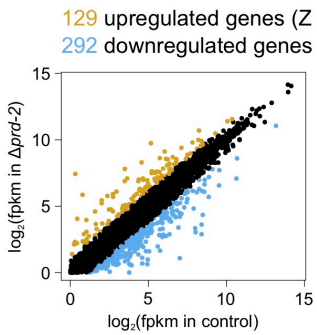

Downregulated genes -> FunCat

FunCat ID	Category description	Adjusted p-value	# genes / category	# genes / input
01.05.03	polysaccharide metabolism	2.61×10^{-9}	25 / 229	25 / 128
1.05	C-compound and carbohydrate metabolism	3.58×10^{-9}	44 / 711	44 / 128
1.2	secondary metabolism	2.38×10^{-7}	33 / 497	33 / 128
01.05.02.07	sugar, glucoside, polyol and carboxylate catabolism	6.12×10^{-6}	18 / 191	18 / 128

Upregulated genes -> FunCat

FunCat ID	Category description	Adjusted p-value	# genes / category	# genes / input
32.07.03	detoxification by modification	2.16×10^{-3}	6 / 39	6 / 80
16.21.17	pyridoxal phosphate binding	2.21×10^{-3}	6 / 44	6 / 80
1.01	amino acid metabolism	2.85×10^{-3}	11 / 192	11 / 80
2.01	glycolysis and gluconeogenesis	2.85×10^{-3}	7 / 75	7 / 80

Supplementary Figure 4. Hundreds of genes have altered expression levels in the Δ*prd-2* mutant but a common pathway or sequence motif was not detected. RNA-Seq data were first filtered for low expression. 8,622 out of 9,730 annotated *N. crassa* genes were expressed in 4/6 samples (> 0 FPKM units in triplicate control and Δ*prd-2*). FPKM units for 8,622 expressed genes were $\log_2$-transformed, averaged, subtracted from control, and Z-scores computed. 129 genes (gold) were upregulated in Δ*prd-2* (Z-score < -2), and 292 genes (blue) were downregulated in Δ*prd-2* (Z-score > 2). Hypothesizing that PRD-2 is an RNA-binding protein that stabilizes its target transcripts (Figure 3B), we searched for enriched sequence motifs in the untranslated regions of the 292 downregulated genes using Weeder2 (212 annotated 5' UTRs and 226 annotated 3' UTRs searched). Zero motifs scored better than 1.5 from Weeder2 output compared to background *Neurospora* nucleotide frequencies (data not shown). Up- and down-regulated gene categories were then run through FunCat to determine functionally enriched categories of genes in the putative PRD-2 regulon. 128 of the 292 downregulated genes were input to FunCat, and the top scoring functional categories indicated that carbohydrate and secondary metabolism were decreased in Δ*prd-2*. 80 out of the 128 upregulated genes were also input to FunCat, and other metabolism categories were identified, which could indicate altered central carbon metabolism in the Δ*prd-2* mutant, correlating with its slow growth phenotype.

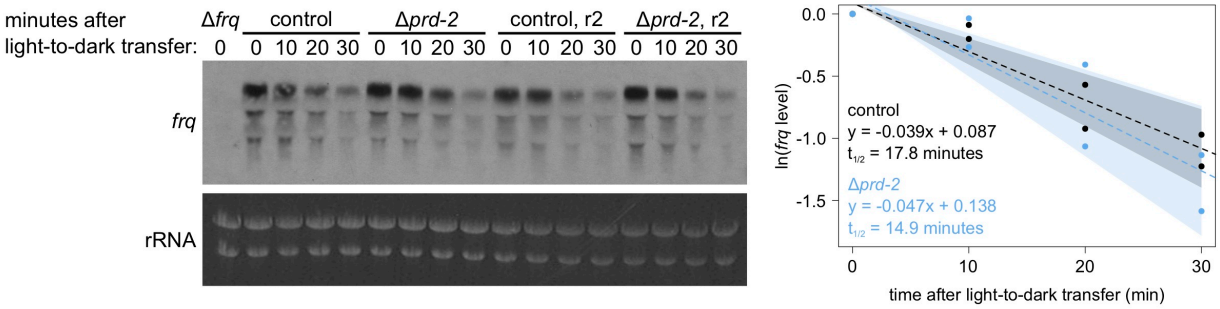

741

742 **Supplementary Figure 5. Loss of *prd*-2 has little effect on stability of the *frq* transcript.** *frq*
743 mRNA degradation kinetics were examined by Northern blot in a time course after light-to-dark
744 transfer (N = 2 biological replicates). RNA levels were quantified using ImageJ, natural log
745 transformed, fit with a linear model (`glm` in R, Gaussian family defaults), and half-life was
746 calculated assuming first order decay kinetics (ln(2) / slope). Shaded areas around the linear fit
747 represent 95% confidence intervals on the slope. The *frq* half-life is approximately 3 minutes
748 shorter in Δ*prd-2* but is not statistically different from the control.

749

750

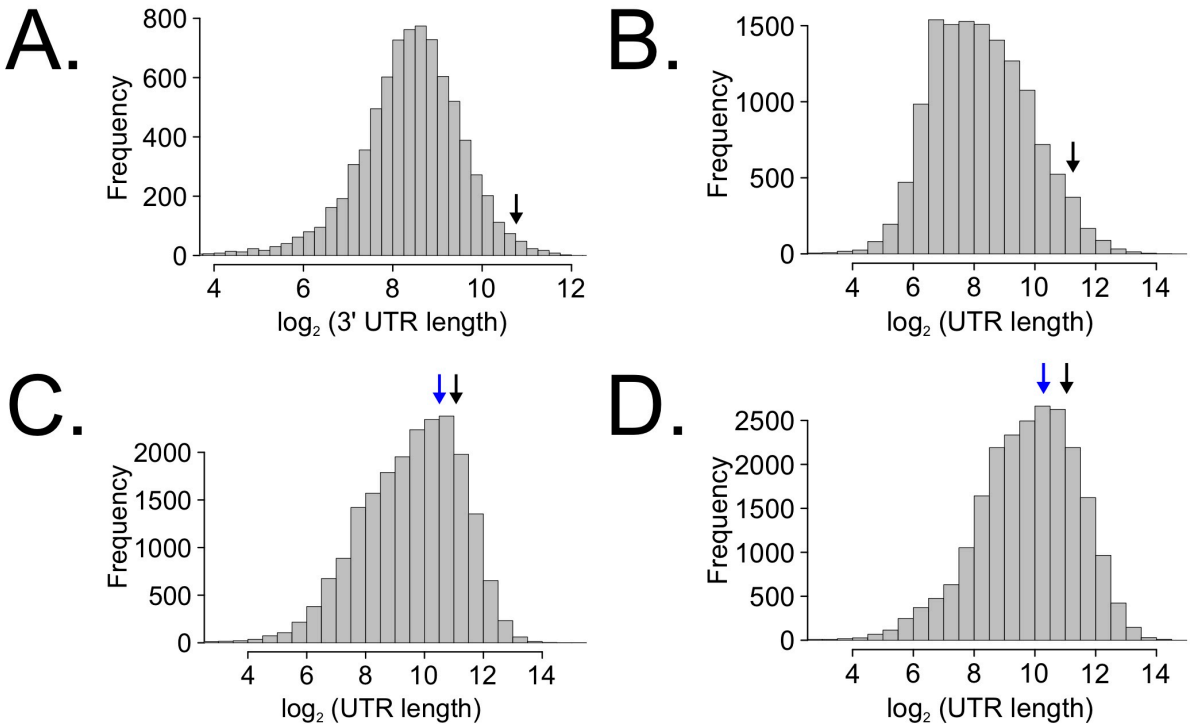

751

752 **Supplementary Figure 6. Long untranslated regions (UTRs) are characteristic of *casein***
753 ***kinase I* gene orthologs across species.** *Neurospora* 3' UTR lengths were mined from 7,793
754 annotated genes (as described in Figure 5C) and plotted as a histogram. The black arrow marks

the 3' UTR of *ck-1a* (NCU00685) at 1,739 bp in length (**A**). UTR lengths from *Drosophila melanogaster* were mined from 13,552 uniquely annotated genes (Ensembl GTF version BDGP6, accessed on 8/5/2020 from Illumina iGenomes) and plotted as a histogram. The black arrow marks the UTR of *dbt* (FBgn0002413) at 2,443 bp in length (**B**). UTR lengths from *Mus musculus* were mined from 20,477 uniquely annotated genes (Ensembl GTF version GRCm38, accessed on 8/5/2020 from Illumina iGenomes) and plotted as a histogram. The black arrow marks the UTR of CSNK1D (ENSMUSG00000025162) at 2,157 bp in length, and the blue arrow corresponds to CSNK1E (ENSMUSG00000022433) at 1,456 bp (**C**). UTR lengths from *Homo sapiens* were mined from 22,401 uniquely annotated genes (Ensembl GTF version GRCh37, accessed on 8/5/2020 from Illumina iGenomes) and plotted as a histogram. The black arrow marks the UTR of CSNK1D (ENSG00000141551) at 2,113 bp in length, and the blue arrow corresponds to CSNK1E (ENSG00000213923) at 1,247 bp (**D**).

Supplementary Table 1. *Neurospora crassa* strains used in this study.

Strain	Genotype	Source
FGSC2489	OR74A *mat* A	FGSC
FGSC9718	Δ*mus-51*::bar^R; *mat* a	FGSC
FGSC11229	ΔNCU04242::hph^R; *mat* a	FGSC (*prd-6*)
FGSC15706	ΔNCU05267::hph^R; Δ*mus-51*::bar^R; *mat* a	FGSC (*upf2*)
FGSC11679	ΔNCU03435::hph^R; *mat* a	FGSC (*upf3*)
FGSC12475	ΔNCU03775::hph^R; *mat* A	FGSC
87-3	*ras-1^{bd}*; *mat* a	This Laboratory
328-4	*ras-1^{bd}*; *mat* A	This Laboratory
613-43	*ras-1^{bd}*; *prd-2*; *mat* a	Feldman Laboratory
613-102	*ras-1^{bd}*; *prd-2*; *mat* A	Feldman Laboratory
1138-1	[bar^R::*qa-2*p-NCU00685]; Δmus-52::hph^R; *ras-1^{bd}*; *mat* a [heterokaryon]	PMID: 19450520
1810	*ras-1^{bd}*; ΔNCU01019::bar^R; *mat* A	This Study (Fig 1, 3, 4)
834-1	*ras-1^{bd}*; hph^R::*qa-2*p-NCU01019	This Study (Fig 1)
1929	*csr-1*::NCU01019-luciferase; *ras-1^{bd}*; *prd-2^{INV}*; *mat* A	This Study (Fig 1)
1930	*csr-1*::NCU01019-luciferase; *ras-1^{bd}*; *mat* A	This Study (Sup Fig 2)
1786-1	*csr-1*::*frq*$_{cbox}$p-luciferase::bar^R; *ras-1^{bd}*; *mat* a	This Study (Fig 2, 4, 5)
1931	*csr-1*::*frq*$_{cbox}$p-luciferase::bar^R; *ras-1^{bd}*; ΔNCU01019::bar^R; *mat* A	This Study (Fig 2, 4, 5)
1932	*csr-1*::*frq*$_{cbox}$p-luciferase::bar^R; *ras-1^{bd}*; V5-NCU01019ΔSUZ[Δaa345-431]::hph^R	This Study (Fig 2)
1933	*csr-1*::*frq*$_{cbox}$p-luciferase::bar^R; *ras-1^{bd}*; V5-NCU01019ΔCterminus[Δaa440-790]::hph^R	This Study (Fig 2)
1934	*csr-1*::*frq*$_{cbox}$p-luciferase::bar^R; Δ*mus-51*::bar^R; NCU01019ΔR3H[Δaa264-344]::hph^R	This Study (Fig 2)

CX002_B4-11-1	*csr-1*::NCU01019ΔSUZ[Δaa345-432]-V5::bar^R; *ras-1^{bd}*; ΔNCU01019::hph^R	This Study (Fig 2)
CX002_B4-11-6	*csr-1*::NCU01019ΔR3H[Δaa281-344]-V5::bar^R; *ras-1^{bd}*; ΔNCU01019::hph^R	This Study (Fig 2)
CX002_B4-11-5	*csr-1*::NCU01019ΔCterminus[Δaa495-790]-V5::bar^R; *ras-1^{bd}*; ΔNCU01019::hph^R	This Study (Fig 2)
CX002_B4-11-3	*csr-1*::NCU01019ΔCterminus[Δaa525-612]-V5::bar^R; *ras-1^{bd}*; ΔNCU01019::hph^R	This Study (Fig 2)
CX002_B4-11-8	*csr-1*::NCU01019ΔCterminus[Δaa625-682]-V5::bar^R; *ras-1^{bd}*; ΔNCU01019::hph^R	This Study (Fig 2)
1813	*ras-1^{bd}*; NCU01019-10xGly_V5_10xHis_3xFLAG::hph^R; *mat* a	This Study (Fig 2, 3)
1888	*ras-1^{bd}*; NCU16560-10xGly_V5_10xHis_3xFLAG::hph^R	This Study (Fig 3)
1935	bar^R::*qa-2*p-NCU00685; *ras-1^{bd}*	This Study (Fig 4, 5)
1936	bar^R::*qa-2*p-NCU00685; *ras-1^{bd}*; ΔNCU01019::bar^R	This Study (Fig 4)
721-3	NCU00685-SHORT-HA3::hph^R; *ras-1^{bd}*; *mat* a	This Study
1937	*csr-1*::*frq*$_{cbox}$p-luciferase::bar^R; NCU00685-SHORT-HA3::hph^R; *ras-1^{bd}*; *mat* a	This Study (Fig 4)
1938	*csr-1*::*frq*$_{cbox}$p-luciferase::bar^R; NCU00685-SHORT-HA3::hph^R; *ras-1^{bd}*; ΔNCU01019::bar^R	This Study (Fig 4)
1939	*csr-1*::*frq*$_{cbox}$p-luciferase::bar^R; *ras-1^{bd}*; ΔNCU04242::hph^R; *mat* A	This Study (Fig 5)
1940	*csr-1*::*frq*$_{cbox}$p-luciferase::bar^R; *ras-1^{bd}*; ΔNCU01019::bar^R; ΔNCU04242::hph^R	This Study (Fig 5)
1941	*csr-1*::*frq*$_{cbox}$p-luciferase::bar^R; *ras-1^{bd}*; ΔNCU05267::hph^R	This Study (Fig 5)
1942	*csr-1*::*frq*$_{cbox}$p-luciferase::bar^R; *ras-1^{bd}*; ΔNCU05267::hph^R; ΔNCU01019::bar^R	This Study (Fig 5)
1943	*csr-1*::*frq*$_{cbox}$p-luciferase::bar^R; ΔNCU03435::hph^R; *ras-1^{bd}*	This Study (Fig 5)
1944	*csr-1*::*frq*$_{cbox}$p-luciferase::bar^R; ΔNCU03435::hph^R; *ras-1^{bd}*; ΔNCU01019::bar^R	This Study (Fig 5)
1945	bar^R::*qa-2*p-NCU00685; *ras-1^{bd}*; ΔNCU04242::hph^R	This Study (Fig 5)

Acknowledgements

We thank the Fungal Genetics Stock Center (Kansas City, Missouri, USA) for curating *N. crassa* strains. We thank Arun Mehra for discussions on preliminary work to identify the clock-relevant mechanism of the *prd-6* mutation, Bin Wang for assistance in constructing and validating the CKI^{SHORT} hyperactive allele, Jill Emerson for assistance in constructing Δ*prd-2* (NCU01019), and Brad Bartholomai for discussions on *prd-2*. The *Neurospora* CK1a antibody was courtesy of Michael Brunner (University of Heidelberg).

Competing Interests

The authors declare that no competing interests exist.

References

Aronson BD, Johnson KA, Loros JJ, Dunlap JC. 1994. Negative feedback defining a circadian clock: autoregulation of the clock gene *frequency*. Science, 263(5153), 1578–84. doi:10.1126/science.8128244

Aryal RP, Kwak PB, Tamayo AG, Gebert M, Chiu PL, Walz T, Weitz CJ. 2017. Macromolecular

787 Assemblies of the Mammalian Circadian Clock. Molecular Cell, 67(5), 770-782.e6.
788 doi:10.1016/j.molcel.2017.07.017
789 Baker CL, Kettenbach AN, Loros JJ, Gerber SA, Dunlap JC. 2009. Quantitative Proteomics
790 Reveals a Dynamic Interactome and Phase-Specific Phosphorylation in the *Neurospora*
791 Circadian Clock. Molecular Cell, 34(3), 354–363. doi:10.1016/j.molcel.2009.04.023
792 Bardiya N, Shiu PKT. 2007. Cyclosporin A-resistance based gene placement system for
793 *Neurospora crassa*. Fungal Genetics and Biology, 44(5), 307–314.
794 doi:10.1016/j.fgb.2006.12.011
795 Belden WJ, Larrondo LF, Froehlich AC, Shi M, Chen CH, Loros JJ, Dunlap JC. 2007. The *band*
796 mutation in *Neurospora crassa* is a dominant allele of *ras-1* implicating RAS signaling in
797 circadian output. Genes & Development, 21(12), 1494–1505. doi:10.1101/gad.1551707
798 Chen CH, Ringelberg CS, Gross RH, Dunlap JC, Loros JJ. 2009. Genome-wide analysis of
799 light-inducible responses reveals hierarchical light signalling in *Neurospora*. The EMBO
800 Journal, 28(8), 1029–1042. doi:10.1038/emboj.2009.54
801 Cheong JK, Virshup DM. 2011. Casein kinase 1: Complexity in the family. International Journal
802 of Biochemistry and Cell Biology, 43(4), 465–469. doi:10.1016/j.biocel.2010.12.004
803 Colot HV, Loros JJ, Dunlap JC. 2005. Temperature-modulated alternative splicing and promoter
804 use in the circadian clock gene *frequency*. Molecular Biology of the Cell, 16(12), 5563–71.
805 doi:10.1091/mbc.E05-08-0756
806 Compton J. 2003. Advances in understanding the molecular biology of *Neurospora crassa*.
807 Ph.D. Thesis, University of California Santa Cruz.
808 Diernfellner ACR, Schafmeier T, Merrow MW, Brunner M. 2005. Molecular mechanism of
809 temperature sensing by the circadian clock of *Neurospora crassa*. Genes & Development,
810 19(17), 1968–1973. doi:10.1101/gad.345905.clock
811 Dobin A, Davis CA, Schlesinger F, Drenkow J, Zaleski C, Jha S, Batut P, Chaisson M, Gingeras
812 TR. 2013. STAR: Ultrafast universal RNA-seq aligner. Bioinformatics, 29(1), 15–21.
813 doi:10.1093/bioinformatics/bts635
814 Dunlap JC, Loros JJ. 2018. Just-So Stories and Origin Myths: Phosphorylation and Structural
815 Disorder in Circadian Clock Proteins. Molecular Cell, 69(2), 165–168.
816 doi:10.1016/j.molcel.2017.11.028
817 Emerson JM, Bartholomai BM, Ringelberg CS, Baker SE, Loros JJ, Dunlap JC. 2015. *period-1*
818 encodes an ATP-dependent RNA helicase that influences nutritional compensation of the
819 *Neurospora* circadian clock. Proceedings of the National Academy of Sciences of the
820 United States of America, 112(51), 15707–15712. doi:10.1073/pnas.1521918112

821 Feldman JF, Hoyle MN. 1973. Isolation of circadian clock mutants of *Neurospora crassa*.
822 Genetics, 75(4), 605–613.
823 Feldman JF, Hoyle MN. 1976. Complementation analysis of linked circadian clock mutants of
824 *Neurospora crassa*. Genetics, 82(1), 9–17.
825 Fustin JM, Kojima R, Itoh K, Chang HY, Ye S, Zhuang B, Oji A, Gibo S, Narasimamurthy R,
826 Virshup D, Kurosawa G, Doi M, Manabe I, Ishihama Y, Ikawa M, Okamura H. 2018. Two
827 *Ck1δ* transcripts regulated by m6A methylation code for two antagonistic kinases in the
828 control of the circadian clock. Proceedings of the National Academy of Sciences of the
829 United States of America, 115(23), 5980–5985. doi:10.1073/pnas.1721371115
830 Garceau NY, Liu Y, Loros JJ, Dunlap JC. 1997. Alternative initiation of translation and time-
831 specific phosphorylation yield multiple forms of the essential clock protein FREQUENCY.
832 Cell, 89(3), 469–476. doi:10.1016/S0092-8674(00)80227-5
833 Gardner GF, Feldman JF. 1981. Temperature Compensation of Circadian Period Length in
834 Clock Mutants of *Neurospora crassa*. Plant Physiology, 68(6), 1244–8. doi:
835 10.1104/pp.68.6.1244
836 Ge Z, Quek BL, Beemon KL, Hogg JR. 2016. Polypyrimidine tract binding protein 1 protects
837 mRNAs from recognition by the nonsense-mediated mRNA decay pathway. eLife, 5, 1–25.
838 doi:10.7554/elife.11155
839 Gooch VD, Mehra A, Larrondo LF, Fox J, Touroutoutoudis M, Loros JJ, Dunlap JC. 2008. Fully
840 codon-optimized *luciferase* uncovers novel temperature characteristics of the *Neurospora*
841 clock. Eukaryotic Cell, 7(1), 28–37. doi:10.1128/EC.00257-07
842 Gorl M, Merrow M, Huttner B, Johnson J, Roenneberg T, Brunner M. 2001. A PEST-like
843 element in FREQUENCY determines the length of the circadian period in *Neurospora*
844 *crassa*. EMBO Journal, 20(24), 7074–7084. doi:10.1093/emboj/20.24.7074
845 Guo G, Wang K, Hu SS, Tian T, Liu P, Mori T, Chen P, Johnson CH, Qin X. 2019. Autokinase
846 Activity of Casein Kinase 1 δ/ε Governs the Period of Mammalian Circadian Rhythms.
847 Journal of Biological Rhythms, 34(5), 482–496. doi:10.1177/0748730419865406
848 Guo J, Cheng P, Yuan H, Liu Y. 2009. The Exosome Regulates Circadian Gene Expression in a
849 Posttranscriptional Negative Feedback Loop. Cell, 138(6), 1236–1246.
850 doi:10.1016/j.cell.2009.06.043
851 He Q, Cha J, He Q, Lee HC, Yang Y, Liu Y. 2006. CKI and CKII mediate the FREQUENCY-
852 dependent phosphorylation of the WHITE COLLAR complex to close the *Neurospora*
853 circadian negative feedback loop. Genes & Development, 20(18), 2552–2565.
854 doi:10.1101/gad.1463506

Heintzen C, Loros JJ, Dunlap JC. 2001. The PAS protein VIVID defines a clock-associated feedback loop that represses light input, modulates gating, and regulates clock resetting. Cell, 104(3), 453–464. doi:10.1016/S0092-8674(01)00232-X

Hong CI, Ruoff P, Loros JJ, Dunlap JC. 2008. Closing the circadian negative feedback loop: FRQ-dependent clearance of WC-1 from the nucleus. Genes & Development, 22(22), 3196–3204. doi:10.1101/gad.1706908

Hurley JM, Dasgupta A, Emerson JM, Zhou X, Ringelberg CS, Knabe N, Lipzen AM, Lindquist EA, Daum CG, Barry KW, Grigoriev IV, Smith KM, Galagan JE, Bell-Pedersen D, Freitag M, Cheng C, Loros JJ, Dunlap JC. 2014. Analysis of clock-regulated genes in *Neurospora* reveals widespread posttranscriptional control of metabolic potential. Proceedings of the National Academy of Sciences of the United States of America, 111(48), 16995–17002. doi:10.1073/pnas.1418963111

Hurley JM, Jankowski MS, De Los Santos H, Crowell AM, Fordyce SB, Zucker JD, Kumar N, Purvine SO, Robinson EW, Shukla A, Zink E, Cannon WR, Baker SE, Loros JJ, Dunlap JC. 2018. Circadian Proteomic Analysis Uncovers Mechanisms of Post-Transcriptional Regulation in Metabolic Pathways. Cell Systems, 7(6), 613-626.e5. doi:10.1016/j.cels.2018.10.014

Hurley JM, Larrondo LF, Loros JJ, Dunlap JC. 2013. Conserved RNA helicase FRH acts nonenzymatically to support the intrinsically disordered *Neurospora* clock protein FRQ. Molecular Cell, 52(6), 832–843. doi:10.1016/j.molcel.2013.11.005

Hurley JM, Loros JJ, Dunlap JC. 2016. Circadian Oscillators: Around the Transcription-Translation Feedback Loop and on to Output. Trends in Biochemical Sciences, 41(10), 834–846. doi:10.1016/j.tibs.2016.07.009

Isojima Y, Nakajima M, Ukai H, Fujishima H, Yamada RG, Masumoto KH, Kiuchi R, Ishida M, Ukai-Tadenuma M, Minami Y, Kito R, Nakao K, Kishimoto W, Yoo SH, Shimomura K, Takao T, Takano A, Kojima T, Nagai K, Sakaki Y, Takahashi JS, Ueda HR. 2009. CKIepsilon/delta-dependent phosphorylation is a temperature-insensitive, period-determining process in the mammalian circadian clock. Proceedings of the National Academy of Sciences of the United States of America, 106(37), 15744–9. doi:10.1073/pnas.0908733106

James AB, Syed NH, Bordage S, Marshall J, Nimmo GA, Jenkins GI, Herzyk P, Brown JW, Nimmo HG. 2012. Alternative splicing mediates responses of the *Arabidopsis* circadian clock to temperature changes. Plant Cell, 24(3), 961–981. doi:10.1105/tpc.111.093948

Kelliher CM, Loros JJ, Dunlap JC. 2020. Evaluating the circadian rhythm and response to

889 glucose addition in dispersed growth cultures of *Neurospora crassa*. Fungal Biology,
890 124(5), 398–406. doi:10.1016/j.funbio.2019.11.004
891 Kloss B, Rothenfluh A, Young MW, Saez L. 2001. Phosphorylation of PERIOD is influenced by
892 cycling physical associations of DOUBLE-TIME, PERIOD, and TIMELESS in the
893 *Drosophila* clock. Neuron, 30(3), 699–706. doi:10.1016/S0896-6273(01)00320-8
894 Koike N, Yoo SH, Huang HC, Kumar V, Lee C, Kim TK, Takahashi JS. 2012. Transcriptional
895 architecture and chromatin landscape of the core circadian clock in mammals. Science,
896 338(6105), 349–54. doi:10.1126/science.1226339
897 Konopka RJ, Benzer S. 1971. Clock mutants of *Drosophila melanogaster*. Proceedings of the
898 National Academy of Sciences of the United States of America, 68(9), 2112–6.
899 doi:10.1073/pnas.68.9.2112
900 Kramer C, Loros JJ, Dunlap JC, Crosthwaite SK. 2003. Role for antisense RNA in regulating
901 circadian clock function in *Neurospora crassa*. Nature Biotechnology, 421(6926), 948–952.
902 doi:10.1038/nature01427
903 Lambreghts R. 2012. Exploring New Players in the *Neurospora* Core Clock and its Output.
904 Ph.D. Thesis, Dartmouth College, 1–335.
905 Larrondo LF, Olivares-Yañez C, Baker CL, Loros JJ, Dunlap JC. 2015. Decoupling circadian
906 clock protein turnover from circadian period determination. Science, 347(6221), 1257277-
907 1–8. doi:10.1126/science.1257277
908 Lauinger L, Li J, Shostak A, Cemel IA, Ha N, Zhang Y, Merkl PE, Obermeyer S, Stankovic-
909 Valentin N, Schafmeier T, Wever WJ, Bowers AA, Carter KP, Palmer AE, Tschochner H,
910 Melchior F, Deshaies RJ, Brunner M, Diernfellner A. 2017. Thiolutin is a zinc chelator that
911 inhibits the Rpn11 and other JAMM metalloproteases. Nature Chemical Biology, 13(7),
912 709–714. doi:10.1038/nchembio.2370
913 Lee H, Chen R, Lee Y, Yoo S, Lee C. 2009. Essential roles of CKIδ and CKIε in the mammalian
914 circadian clock. Proceedings of the National Academy of Sciences, 106(50), 21359–21364.
915 doi:10.1073/pnas.0906651106
916 Lewis M. 1995. Molecular genetic analysis of circadian clock genes in *Neurospora crassa*. Ph.D.
917 Thesis, University of California Santa Cruz.
918 Liu X, Chen A, Caicedo-Casso A, Cui G, Du M, He Q, Lim S, Kim HJ, Hong CI, Liu Y. 2019.
919 FRQ-CK1 interaction determines the period of circadian rhythms in *Neurospora*. Nature
920 Communications, 10(1), 1–13. doi:10.1038/s41467-019-12239-w
921 Liu Y, Garceau NY, Loros JJ, Dunlap JC. 1997. Thermally regulated translational control of FRQ
922 mediates aspects of temperature responses in the *Neurospora* circadian clock. Cell, 89(3),

477–486. doi:10.1016/S0092-8674(00)80228-7

Loros JJ. 2020. Principles of the animal molecular clock learned from *Neurospora*. European Journal of Neuroscience, 51(1), 19–33. doi: 10.1111/ejn.14354

Majercak J, Sidote D, Hardin PE, Edery I. 1999. How a circadian clock adapts to seasonal decreases in temperature and day length. Neuron, 24(1), 219–230. doi:10.1016/S0896-6273(00)80834-X

Mateos JL, de Leone MJ, Torchio J, Reichel M, Staiger D. 2018. Beyond transcription: Fine-tuning of circadian timekeeping by post-transcriptional regulation. Genes, 9(12). doi:10.3390/genes9120616

Mehra A, Shi M, Baker CL, Colot HV, Loros JJ, Dunlap JC. 2009. A Role for Casein Kinase 2 in the Mechanism Underlying Circadian Temperature Compensation. Cell, 137(4), 749–760. doi:10.1016/j.cell.2009.03.019

Metzenberg RL. 2004. Bird Medium: an alternative to Vogel Medium. Fungal Genetics Reports, 51, 19–20. doi:10.4148/1941-4765.1138

Millius A, Ueda HR. 2017. Systems biology-derived discoveries of intrinsic clocks. Frontiers in Neurology, 8, 1–19. doi:10.3389/fneur.2017.00025

Morgan LW, Feldman JF. 1997. Isolation and characterization of a temperature-sensitive circadian clock mutant of *Neurospora crassa*. Genetics, 146(2), 525–30.

Morgan LW, Feldman JF. 2001. Epistatic and synergistic interactions between circadian clock mutations in *Neurospora crassa*. Genetics, 159(2), 537–543.

Nakashima H. 1981. A liquid culture method for the biochemical analysis of the circadian clock of *Neurospora crassa*. Plant & Cell Physiology, 22(2), 231–238.

Narasimamurthy R, Hunt SR, Lu Y, Fustin JM, Okamura H, Partch CL, Forger DB, Kim JK, Virshup DM. 2018. CK1δ/e protein kinase primes the PER2 circadian phosphoswitch. Proceedings of the National Academy of Sciences of the United States of America, 115(23), 5986–5991. doi:10.1073/pnas.1721076115

Ode KL, Ukai H, Susaki EA, Narumi R, Matsumoto K, Hara J, Koide N, Abe T, Kanemaki MT, Kiyonari H, Ueda HR. 2017. Knockout-Rescue Embryonic Stem Cell-Derived Mouse Reveals Circadian-Period Control by Quality and Quantity of CRY1. Molecular Cell, 65(1), 176–190. doi:10.1016/j.molcel.2016.11.022

Partch CL. 2020. Orchestration of Circadian Timing by Macromolecular Protein Assemblies. Journal of Molecular Biology, 432(12), 3426–3448. doi:10.1016/j.jmb.2019.12.046

Pelham JF, Dunlap JC, Hurley JM. 2020. Intrinsic disorder is an essential characteristic of components in the conserved circadian circuit. Cell Communication and Signaling, In

957 Press.
958 Pelham JF, Mosier AE, Hurley JM. 2018. Characterizing Time-of-Day Conformational Changes
959 in the Intrinsically Disordered Proteins of the Circadian Clock. Methods in Enzymology,
960 611, 503–529. doi:10.1016/bs.mie.2018.08.024
961 Philpott JM, Narasimamurthy R, Ricci CG, Freeberg AM, Hunt SR, Yee LE, Pelofsky RS,
962 Tripathi S, Virshup DM, Partch CL. 2020. Casein kinase 1 dynamics underlie substrate
963 selectivity and the PER2 circadian phosphoswitch. eLife, 9, 1–28. doi:10.7554/eLife.52343
964 Pregueiro AM, Liu Q, Baker CL, Dunlap JC, Loros JJ. 2006. The *Neurospora* checkpoint kinase
965 2: a regulatory link between the circadian and cell cycles. Science, 313(5787), 644–9.
966 doi:10.1126/science.1121716
967 Querfurth C, Diernfellner A, Heise F, Lauinger L, Neiss A, Tataroglu Ö, Brunner M, Schafmeier
968 T. 2007. Posttranslational regulation of *Neurospora* circadian clock by CK1a-dependent
969 phosphorylation. Cold Spring Harbor Symposia on Quantitative Biology, 72, 177–183.
970 doi:10.1101/sqb.2007.72.025
971 Ralph MR, Menaker M. 1988. A mutation of the circadian system in golden hamsters. Science,
972 241(4870), 1225–1227. doi:10.1126/science.3413487
973 Ri H, Lee J, Sonn JY, Yoo E, Lim C, Choe J. 2019. *Drosophila CrebB* is a Substrate of the
974 Nonsense-Mediated mRNA Decay Pathway that Sustains Circadian Behaviors. Molecules
975 and Cells, 42(4), 301–312. doi:10.14348/molcells.2019.2451
976 Roenneberg T, Taylor W. 2000. Automated recordings of bioluminescence with special
977 reference to the analysis of circadian rhythms. Methods in Enzymology, 305, 104–119. doi:
978 10.1016/s0076-6879(00)05481-1
979 Sargent ML, Briggs WR, Woodward DO. 1966. Circadian nature of a rhythm expressed by an
980 invertaseless strain of *Neurospora crassa*. Plant Physiology, 41(8), 1343–9.
981 doi:10.1104/pp.41.8.1343
982 Song MH, Aravind L, Müller-Reichert T, O'Connell KF. 2008. The conserved protein SZY-20
983 opposes the Plk4-related kinase ZYG-1 to limit centrosome size. Developmental Cell,
984 15(6), 901–12. doi:10.1016/j.devcel.2008.09.018
985 Sundaram S, Nagaraj S, Mahoney H, Portugues A, Li W, Millsaps K, Faulkner J, Yunus A,
986 Burns C, Bloom C, Said M, Pinto L, Azam S, Flores M, Henriksen A, Gamsby J, Gulick D.
987 2019. Inhibition of casein kinase 1δ/ε improves cognitive-affective behavior and reduces
988 amyloid load in the APP-PS1 mouse model of Alzheimer's disease. Scientific Reports, 9(1),
989 1–13. doi:10.1038/s41598-019-50197-x
990 Tan Y, Dragovic Z, Roenneberg T, Merrow M. 2004. Entrainment dissociates transcription and

translation of a circadian clock gene in *Neurospora*. Current Biology, 14(5), 433–438. doi:10.1016/j.cub.2004.02.035

Toh KL, Jones CR, He Y, Eide EJ, Hinz WA, Virshup DM, Ptácek LJ, Fu YH. 2001. An hPer2 phosphorylation site mutation in familial advanced sleep phase syndrome. Science, 291(5506), 1040–1043. doi:10.1126/science.1057499

Top D, O'Neil JL, Merz GE, Dusad K, Crane BR, Young MW. 2018. CK1/doubletime activity delays transcription activation in the circadian clock. eLife, 7, 1–21. doi:10.7554/eLife.32679

Trapnell C, Hendrickson DG, Sauvageau M, Goff L, Rinn JL, Pachter L. 2013. Differential analysis of gene regulation at transcript resolution with RNA-seq. Nature Biotechnology, 31(1), 46–53. doi:10.1038/nbt.2450

Tsuchiya Y, Umemura Y, Minami Y, Koike N, Hosokawa T, Hara M, et al. 2016. Effect of Multiple Clock Gene Ablations on the Circadian Period Length and Temperature Compensation in Mammalian Cells. Journal of Biological Rhythms, 31(1), 48–56. doi:10.1177/0748730415613888

Vanselow K, Vanselow JT, Westermark PO, Reischl S, Maier B, Korte T, et al. 2006. Differential effects of PER2 phosphorylation: Molecular basis for the human familial advanced sleep phase syndrome (FASPS). Genes and Development, 20(19), 2660–2672. doi:10.1101/gad.397006

Vielhaber E, Virshup DM. 2001. Casein kinase I: From obscurity to center stage. IUBMB Life, 51(2), 73–78. doi:10.1080/15216540152122049

Wang B, Kettenbach AN, Zhou X, Loros JJ, Dunlap JC. 2019. The Phospho-Code Determining Circadian Feedback Loop Closure and Output in *Neurospora*. Molecular Cell, 74(4), 771–784. doi:10.1016/j.molcel.2019.03.003

Weischenfeldt J, Waage J, Tian G, Zhao J, Damgaard I, Jakobsen JS, Kristiansen K, Krogh A, Wang J, Porse BT. 2012. Mammalian tissues defective in nonsense-mediated mRNA decay display highly aberrant splicing patterns. Genome Biology, 13(5). doi:10.1186/gb-2012-13-5-r35

Wilinski D, Buter N, Klocko AD, Lapointe CP, Selker EU, Gasch AP, Wickens M. 2017. Recurrent rewiring and emergence of RNA regulatory networks. Proceedings of the National Academy of Sciences of the United States of America, 114(14), E2816–E2825. doi:10.1073/pnas.1617777114

Wu C, Yang F, Smith KM, Peterson M, Dekhang R, Zhang Y, Zucker J, Bredeweg EL, Mallappa C, Zhou X, Lyubetskaya A, Townsend JP, Galagan JE, Freitag M, Dunlap JC, Bell-

1025 Pedersen D, Sachs MS. 2014. Genome-Wide Characterization of Light-Regulated Genes
1026 in *Neurospora crassa*. G3: Genes|Genomes|Genetics, 4(9), 1731–1745.
1027 doi:10.1534/g3.114.012617
1028 Wu Y, Zhang Y, Sun Y, Yu J, Wang P, Chen S, Ma L, Zhang D, He Q, Guo J. 2017. Up-
1029 Frameshift Protein UPF1 Regulates *Neurospora crassa* Circadian and Diurnal Growth
1030 Rhythms. Genetics, 206(4), 1881–1893. doi: 10.1534/genetics.117.202788
1031 Xu Y, Padiath QS, Shapiro RE, Jones CR, Wu SC, Saigoh N, Saigoh K, Ptácek LJ, Fu YH.
1032 2005. Functional consequences of a CKIδ mutation causing familial advanced sleep phase
1033 syndrome. Nature, 434(7033), 640–644. doi:10.1038/nature03453
1034 Yoo SH, Kojima S, Shimomura K, Koike N, Buhr ED, Furukawa T, Ko CH, Gloston G, Ayoub C,
1035 Nohara K, Reyes BA, Tsuchiya Y, Yoo OJ, Yagita K, Lee C, Chen Z, Yamazaki S, Green
1036 CB, Takahashi JS. 2017. Period2 3′-UTR and microRNA-24 regulate circadian rhythms by
1037 repressing PERIOD2 protein accumulation. Proceedings of the National Academy of
1038 Sciences, 114(42). doi:10.1073/pnas.1706611114
1039 Zhang Y, Sachs MS. 2015. Control of mRNA stability in fungi by NMD, EJC and CBC factors
1040 through 3′UTR introns. Genetics, 200(4), 1133–48. doi:10.1534/genetics.115.176743
1041 Zhou M, Guo J, Cha J, Chae M, Chen S, Barral JM, Sachs MS, Liu Y. 2013. Non-optimal codon
1042 usage affects expression, structure and function of clock protein FRQ. Nature, 495(7439),
1043 111–115. doi:10.1038/nature11833
1044 Zhou M, Kim JK, Eng GWL, Forger DB, Virshup DM. 2015. A Period2 Phosphoswitch Regulates
1045 and Temperature Compensates Circadian Period. Molecular Cell, 60(1), 77–88.
1046 doi:10.1016/j.molcel.2015.08.022
1047